LIGO Laboratory / LIGO Scientific Collaboration

LIGO-T0900325-v2	Advanced LIGO	12/5/11

H1 Squeezer Noise Model

Sheila Dwyer, Sheon Chua, Michael Stefszky, Daniel Sigg, Nergis Mavalvala

Distribution of this document:
LIGO Scientific Collaboration

This is an internal working note
of the LIGO Laboratory.

California Institute of Technology
LIGO Project – MS 18-34
1200 E. California Blvd.
Pasadena, CA 91125
Phone (626) 395-2129
Fax (626) 304-9834
E-mail: info@ligo.caltech.edu

Massachusetts Institute of Technology
LIGO Project – NW22-295
185 Albany St
Cambridge, MA 02139
Phone (617) 253-4824
Fax (617) 253-7014
E-mail: info@ligo.mit.edu

LIGO Hanford Observatory
P.O. Box 159
Richland WA 99352
Phone 509-372-8106
Fax 509-372-8137

LIGO Livingston Observatory
P.O. Box 940
Livingston, LA 70754
Phone 225-686-3100
Fax 225-686-7189

http://www.ligo.caltech.edu

Table of Contents

1 Sensing and Actuation

1.1 Overview

A block diagram of the servo model and noise propagation model is shown in Figure 1: Servo model of the H1 squeezer.Figure 2.

1.2 Main laser

The main laser, f_{Main}, is locked to the fiber output which is taken from the interferometer laser, f_{PSL},. This will guarantee that the squeezer is operating on the correct frequency. In order to lock the phase a feedback path from the local oscillator (S$_3$) adjusts the offset of the frequency stabilization servo (FSS). The error signal expressed as phase angles can be written as

$$V_0^{\phi}(s) = \phi_{Main} - \phi_{PSL} + \phi_0 \tag{1}$$

where ϕ_0 denotes the demodulation angle. One can always do the calculation in phase by simply multiplying the frequency by $1/s$. We absorb the scaling factor due to the light level on the photodetector into the photodetector transfer function

$$S_0(s) = 2\sqrt{\eta_{PSL,0}P_{PSL}\eta_{Main,0}P_{Main}}\,\eta_{QE,0}\varepsilon_R Z_0 \tag{2}$$

where P_{PSL}, P_{Main}, η_{QE}, ε_R, Z_0 denote the light available from the PSL, the light power of the main laser, the photodetector quantum efficiency, the photodetector responsivity, and the photodetector transimpedance gain. The factor $\eta_{PSL,0}$ and $\eta_{Main,0}$ are the attenuation factors of the two interfering beams, respectively, and account for beamsplitter ratios and attenuators.

1.3 Auxiliary laser

The auxiliary laser is used to generate a frequency shifted subcarrier which is used for coherent locking of the squeezer phase to main interferometer beam at the antisymmetric port. It deploys a second FFS. The offset point into the error signal of the servo can be used as a fast feedback for the phase angle between the green pump beam into the OPO and the coherent field. The error signal and photodetector transfer function are identical to the ones from the main laser:

$$V_1^{\phi}(s) = \phi_{Aux} - \phi_{Main} + \phi_1 \tag{3}$$

where ϕ_1 denotes the demodulation angle. We absorb the scaling factor to the light levels into the photodetector transfer function

$$S_1(s) = 2\sqrt{\eta_{Main,1}P_{Main}\eta_{Aux,1}P_{Aux}}\,\eta_{QE,1}\varepsilon_R Z_1 \tag{4}$$

where Z_1 denotes the photodetector transimpedance gain. The factors $\eta_{Main,1}$ and $\eta_{Aux,1}$ again account for the beam attenuation in each interfering beam, respectively.
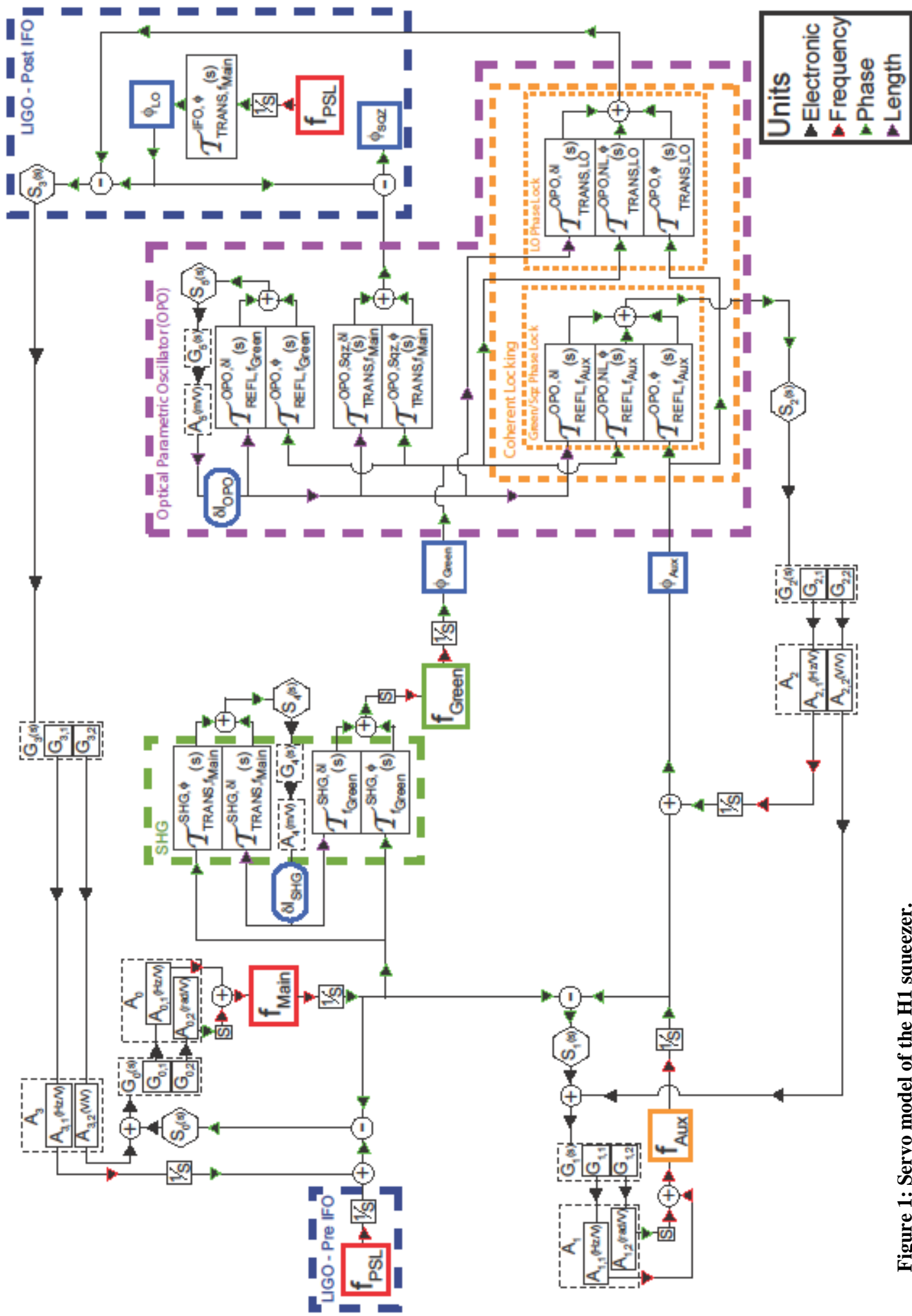
Figure 1: Servo model of the H1 squeezer.

1.4 SHG

The SHG is locked using a Pound-Drever-Hall signal in transmission of the cavity. For the red light we get the following formulae:

$$T_{TRANS,fMain}^{SHG,\phi}(s) = g_{SR,TRANS} \frac{s}{2\pi f_{S,FSR}} \tag{5}$$

$$T_{TRANS,fMain}^{SHG,\delta l}(s) = g_{SR,TRANS} \frac{k/\pi}{1 + s/2\pi f_{SR}} \tag{6}$$

with

$$k = \frac{2\pi}{\lambda_R} \tag{7}$$

$$g_{SR,TRANS} = -4J_0(\Gamma_{S,M})J_1(\Gamma_{S,M})F_{SR}\sqrt{r_{SR,1}r_{SR,2}\sqrt{1-\delta_{SR}}}\,|t_{SR,SB}\,t_{SR,CR}| \tag{8}$$

$$t_{SR,SB} = \frac{\sqrt{1-\delta_{SR}}\sqrt{1-r_{SR,1}^2}\sqrt{1-r_{SR,2}^2}}{1 - e^{2\pi i f_{S,M}/f_{S,FSR}} r_{SR,1}r_{SR,2}\sqrt{1-\delta_{SR}}} \tag{9}$$

$$t_{SR,CR} = \frac{\sqrt{1-\delta_{SR}}\sqrt{1-r_{SR,1}^2}\sqrt{1-r_{SR,2}^2}}{1 - r_{SR,1}r_{SR,2}\sqrt{1-\delta_{SR}}} \tag{10}$$

$$F_{SR} = \frac{\pi\sqrt{r_{SR,1}r_{SR,2}\sqrt{1-\delta_{SR}}}}{1 - r_{SR,1}r_{SR,2}\sqrt{1-\delta_{SR}}} \tag{11}$$

$$f_{SR} = \frac{f_{S,FSR}}{2F_{SR}} \tag{12}$$

With the parameters from Table 2 we get

$$|t_{SR,CR}|^2 \approx 1.3 \times 10^{-2} \quad \text{and} \quad |t_{SR,SB}|^2 \approx 6.4 \times 10^{-3} \tag{13}$$

For the green output light we get:

$$T_{fGreen}^{SHG,\phi}(s) = \frac{2}{1 + s/2\pi \bar{f}_{SR}} \tag{14}$$

$$T_{fGreen}^{SHG,\delta l}(s) = -4F_{SR}\sqrt{r_{SR,1}r_{SR,2}\sqrt{1-\delta_{SR}}}\,\frac{k/\pi}{1 + s/2\pi f_{SR}} \tag{15}$$

with

$$\bar{f}_{SR} = \frac{f_{SR}}{\sqrt{r_{SR,1}r_{SR,2}\sqrt{1-\delta_{SR}}}} \tag{16}$$

1.5 OPO

The OPO is locked in reflection using the green light. The locking signals can be written as

$$T_{REFL,fGreen}^{OPO,\phi}(s) = g_{OG,REFL} \frac{s}{2\pi f_{O,FSR}} \tag{17}$$

$$T_{REFL,fGreen}^{OPO,\delta l}(s) = g_{OG,REFL} \frac{2k/\pi}{1 + s/2\pi f_{OG}} \tag{18}$$

with

$$g_{OG,REFL} = -4J_0(\Gamma_{O,M})J_1(\Gamma_{O,M})F_{OG} \frac{1 - r_{OG,1}^2}{1 - r_{OG,1}r_{OG,2}} \sqrt{r_{OG,1}r_{OG,2}} \tag{19}$$

$$F_{OG} = \frac{\pi\sqrt{r_{OG,1}r_{OG,2}}}{1 - r_{OG,1}r_{OG,2}} \tag{20}$$

$$f_{OG} = \frac{f_{O,FSR}}{2F_{OG}} \tag{21}$$

The wave vector in green is twice the one in red. This has been accounted for by an explicit factor of 2 in the equation for the length error signal.

1.6 Squeezed Field

The squeezed field sees first the cavity pole of the green light. After it gets converted to red light it will also see the cavity pole of the red light. We write

$$T_{fMain}^{NL,\phi}(s) = \frac{1}{2} \frac{1}{1 + s/2\pi f_{OG}} \frac{1}{1 + s/2\pi f_{OR}} \tag{22}$$

where the factor one half is due to the conversion. The pole frequency is at

$$f_{OR} = \frac{f_{O,FSR}}{2F_{OR}} \tag{23}$$

A length change in the OPO will change both the green light before it is converted and the resulting red light. The two effects add:

$$\begin{aligned}
T_{fMain}^{NL,\delta l}(s) = &-\frac{2F_{OG}k}{\pi} \sqrt{r_{OG,1}r_{OG,2}} \frac{1}{1 + s/2\pi f_{OG}} \frac{1}{1 + s/2\pi f_{OR}} \\
&-\frac{2F_{OR}k}{\pi} \sqrt{r_{OR,1}r_{OR,2}} \frac{1}{1 + s/2\pi f_{OR}}
\end{aligned} \tag{24}$$

In the first term there is a factor of one half from the conversion and a factor of two from the wave vector which cancel.

1.7 Coherent Locking

We write the auxiliary fields reflected from the cavity as

$$E_{REFL,aux} = E_{fAux}e^{i\omega_{aux}t+i\phi_{aux}} + E_{fAux2}e^{-i\omega_{aux}t+i\phi_{aux2}} \tag{25}$$

The prompt reflected field is given by

$$E_{fAux} = -r_{OR,1} + e^{i\varphi}\frac{t_{OR,1}^2}{e^{i\varphi} - r_{OR,1}r_{OR,2}} \tag{26}$$

whereas the auxiliary field at f_{Aux2} is given by

$$E_{fAux2} = e^{-i\varphi}\frac{t_{OR,1}^2}{(e^{-i\varphi} - r_{OR,1}r_{OR,2})(e^{i\varphi} - r_{OR,1}r_{OR,2})} \tag{27}$$

Measuring the power using a photodetector and demodulating by $\cos\left(2\omega_{aux}t + \phi_M - \frac{\pi}{2}\right)$, we get

$$V^\phi(s) = 2E_{fAux}E_{fAux2}\sin(\phi_{aux2} - \phi_{aux} + \phi_M) \tag{28}$$

Locking at the zero crossing by setting $\phi_M = \phi_{aux} - \phi_{aux2}$, we see that only phase variations will remain to produce an error signal. Phase variations in the coherent locking can be due to phase variations on the green pump light, due to phase variations on the auxiliary laser, due to length variations in the OPO and due to the amplitude variations of the auxiliary laser or the green pump light:

$$T_{REFL,\Delta fAux}^{OPO,NL,\phi}(s) = T_{REFL,fAux2}^{OPO,NL,\phi}(s) = H_{OR,2}(s,-\varphi)H_{OG,2}(s,0) \tag{29}$$

$$T_{REFL,\Delta fAux}^{OPO,\phi}(s) = T_{REFL,fAux2}^{OPO,\phi}(s) - \bar{H}_{OR,2}(s,\varphi) \tag{30}$$

$$T_{REFL,\Delta fAux}^{OPO,\delta l}(s) = T_{REFL,fAux2}^{OPO,\delta l}(s) - \bar{\gamma}_{OR,\delta l}(\varphi)\bar{H}_{OR,1}(s,\varphi) \tag{31}$$

$$T_{REFL,\Delta fAux}^{OPO,NL,\Delta A}(s) = T_{REFL,fAux2}^{OPO,NL,\Delta A}(s) = \gamma_{OR,\Delta A}(-\varphi)\frac{s}{\omega_{O,FSR}}H_{OR,3}(s,-\varphi)H_{OG,2}(s,0) \tag{32}$$

$$T_{REFL,\Delta fAux}^{OPO,\Delta A}(s) = T_{REFL,fAux2}^{OPO,\Delta A}(s) - \bar{\gamma}_{OR,\Delta A}(\varphi)\bar{H}_{OR,3}(s,\varphi) \tag{33}$$

with

$$\begin{aligned}
T_{REFL,fAux2}^{OPO,\phi}(s) = &-H_{OR,2}(s,-\varphi)H_{OR,2}(s,\varphi) \\
&+ \gamma_{OR,\Delta A}(-\varphi)\alpha_{OR,\Gamma}(\varphi)\left(\frac{s}{\omega_{0,FSR}}\right)^2 H_{OR,3}(s,-\varphi)H_{OR,3}(s,\varphi)
\end{aligned} \tag{34}$$

$$\begin{aligned}
T_{REFL,fAux2}^{OPO,\delta l}(s) = &+\gamma_{OR,\delta l}(-\varphi)H_{OR,1}(s,-\varphi) \\
&+ 2\gamma_{OG,\delta l}(0)H_{OR,2}(s,-\varphi)H_{OG,1}(s,0) \\
&- \gamma_{OR,\delta l}(\varphi)H_{OR,2}(s,-\varphi)H_{OR,1}(s,\varphi) \\
&+ \gamma_{OR,\Delta A}(-\varphi)\alpha_{OR,\delta l}(\varphi)\frac{s}{\omega_{O,FSR}}H_{OR,3}(s,-\varphi)H_{OR,3}(s,\varphi)
\end{aligned} \tag{35}$$

$$T_{REFL,fAux2}^{OPO,\Delta A}(s) = +\gamma_{OR,\Delta A}(-\varphi)\frac{s}{\omega_{FSR}}H_{OR,3}(s,-\varphi)H_{OR,2}(s,\varphi)$$
$$- \gamma_{OR,\Delta A}(\varphi)\frac{s}{\omega_{O,FSR}}H_{OR,2}(s,-\varphi)H_{OR,3}(s,\varphi) \qquad (36)$$

The transfer function $T_{REFL,fAux2}^{OPO,NL,\phi}(s)$ has a single term arising from phase fluctuations on f_{Green} directly causing phase fluctuations on f_{Aux2}. The transfer function $T_{REFL,fAux2}^{OPO,\phi}(s)$ has two terms arising from *(i)* a phase shift on f_{Aux} directly causing a phase shift on f_{Aux2}, and *(ii)* from a phase shift on f_{Aux} causing an amplitude modulation on f_{Aux} and hence f_{Aux2} which transfers back into a phase shift on f_{Aux2}. The transfer function $T_{REFL,fAux2}^{OPO,\delta l}(s)$ has four terms arising from *(i)* a length variation causing a phase shift on f_{Aux2}, *(ii)* from a length variation causing a phase shift on f_{Green} and hence f_{Aux2}, *(iii)* from a length variation causing a phase shift on f_{Aux} and hence f_{Aux2}, and *(iv)* from length variations on f_{Aux} causing am amplitude modulation on f_{Aux} and hence f_{Aux2} which transfers back into a phase shift on f_{Aux2}. The transfer function $T_{REFL,fAux2}^{OPO,NL,\Delta A}(s)$ only has a single term coming from amplitude variations on f_{Green} causing amplitude variations on f_{fAux2} which translate into phase variations. The transfer function $T_{REFL,fAux2}^{OPO,\Delta A}(s)$ has two terms arising from *(i)* an amplitude variations on f_{Aux} causing amplitude variations on f_{Aux2} which translate into phase variations, and *(ii)* an amplitude variations on f_{Aux} translating into phase variations on f_{Aux} and hence f_{Aux2}. The prompt reflected field f_{Aux} gets contributions to its phase variations from input phase variations, from OPO length variations and from input amplitude variations.

For the auxiliary field, E_{fAux}, entering the OPO we get

$$\left|\frac{\bar{\gamma}_{\delta l}(\varphi)}{\gamma_{\delta l}(\varphi}\right| \approx \frac{1}{16} \quad \text{and} \quad \left|\frac{\bar{\gamma}_{\Delta A}(\varphi)}{\gamma_{\Delta A}(\varphi)}\right| \approx \frac{1}{22} \qquad (37)$$

Or, in other words these terms make a much smaller contribution than the ones carried by E_{fAux2}; and thus we have neglected them.

1.8 Local Oscillator

We write the auxiliary fields transmitted through the OPO cavity as

$$E_{TRANS,aux} = E_{fAux}e^{i\omega_{aux}t+i\phi_{aux}} + E_{fAux2}e^{-i\omega_{aux}t+i\phi_{aux2}} \tag{38}$$

Propagating this field to the anti-symmetric port yields

$$E_{AS} = e^{i\phi_{inj}}E_{TRANS,aux} + E_{LO} \tag{39}$$

where ϕ_{inj} is due to the path length variations in the squeezer injection path, and the local oscillator field is given by

$$E_{LO} = E_{LO}e^{i\phi_{LO}} \tag{40}$$

Demodulating by $\cos(\omega_{aux}t + \phi_M)$ yields

$$W^\phi(s) = + 2E_{LO}E_{fAux}\cos\left(\phi_{aux} + \phi_{inj} - \phi_{LO} - \phi_M\right)$$
$$+ 2E_{LO}E_{fAux2}\cos\left(\phi_{aux2} + \phi_{inj} - \phi_{LO} + \phi_M\right) \tag{41}$$

Setting $\phi_{M,I} = \frac{\phi_{aux} - \phi_{aux2}}{2}$ and $\phi_{M,Q} = \frac{\phi_{aux} - \phi_{aux2} + \pi}{2}$, one gets

$$W_I^\phi(s) = 2E_{LO}\left(E_{fAux} + E_{fAux2}\right)\cos\left(\frac{\phi_{aux} + \phi_{aux2}}{2} + \phi_{inj} - \phi_{LO}\right) \tag{42}$$

$$W_Q^\phi(s) = 2E_{LO}\left(E_{fAux} - E_{fAux2}\right)\sin\left(\frac{\phi_{aux} + \phi_{aux2}}{2} + \phi_{inj} - \phi_{LO}\right) \tag{43}$$

respectively. The non-linear conversion in the OPO will set $\phi_{aux2} = \phi_{green} - \phi_{aux}$, and hence the in-phase photodetector at the anti-symmetric port is sensitive to

$$\phi_{AS} = \phi_{green}/2 + \phi_{inj} - \phi_{LO} + a\left(\phi_{aux} - \frac{\phi_{green}}{2}\right) \tag{44}$$

with a the field amplitude asymmetry

$$a = \frac{E_{fAux} - E_{fAux2}}{E_{fAux} + E_{fAux2}} \tag{45}$$

Again, because we are locked to a zero point, only phase fluctuations enter the measured error signal to first order. Phase variations in the local oscillator locking signal can be due to phase variations on the local oscillator, due to phase variations on the green pump light, due to phase variations on the auxiliary laser, due to length variations in the OPO and due to the amplitude variations of the auxiliary laser or the green pump light:

$$T_{LO}^\phi(s) = -1 \tag{46}$$

$$T_{TRANS,LO}^{OPO,NL,\phi}(s) = \frac{1-a}{2}\,T_{REFL,fAux}^{OPO,NL,\phi}(s) \tag{47}$$

$$T_{TRANS,LO}^{OPO,\phi}(s) = \frac{1-a}{2}T_{REFL,fAux2}^{OPO,\phi} + \frac{1+a}{2}H_{OR,2}(s,\varphi) \tag{48}$$

$$T_{TRANS,LO}^{OPO,\delta l}(s) = \frac{1-a}{2} T_{REFL,fAux2}^{OPO,\delta l}(s) + \frac{1+a}{2} \gamma_{OR,\delta l}(\varphi) H_{OR,1}(s,\varphi) \tag{49}$$

$$T_{TRANS,LO}^{OPO,NL,\Delta A}(s) = \frac{1-a}{2} T_{REFL,fAux2}^{OPO,NL,\Delta A}(s) \tag{50}$$

$$T_{TRANS,LO}^{OPO,\Delta A}(s) = \frac{1-a}{2} T_{REFL,LO}^{OPO,\Delta A}(s) + \frac{1+a}{2} \gamma_{OR,\Delta A}(\varphi) \frac{s}{\omega_{O,FSR}} H_{OR,3}(s,\varphi) \tag{51}$$

The two contributions from each of the sidebands, f_{Aux} and f_{Aux2}, have weighting factors $\frac{1+a}{2}$ and $\frac{1-a}{2}$, respectively. When the sidebands are equal in strength, $a = 0$, any direct contribution from ϕ_{aux} vanishes. In order to be sensitive to the green light phase the amplitude of the f_{Aux2} sideband cannot be zero, i.e. $a < 1$.

The phase of the local oscillator field is related to the phase of the PSL laser by an interferometer transfer function which consists of the mode cleaner pole and the double cavity pole

$$T_{fPSL}^{IFO,\phi}(s) = \frac{1}{1 + s/2\pi f_{MC}} \frac{1}{1 + s/2\pi f_{IFO}} \tag{52}$$

2 Feedback Compensation Networks

2.1 Laser Locking

The laser frequency actuator is a composite between a modulator, a PZT and a heater. The modulator or Pockels cell makes fast feedback up to ~1 MHz possible. The PZT dominates in the low frequency band below a couple of kHz and has a large range. The heater is used at very low frequency below ~1 Hz. Its error signal is usually taken from the PZT control voltage. For this analysis we can neglect the temperature servo all together.

The two actuators can be expressed as

$$A_{0,1} = \frac{2\pi\alpha_{0,1}}{s} \tag{53}$$

$$A_{0,2} = \alpha_{0,2} \tag{54}$$

where $\alpha_{0,2}$ is the response for the modulator in rad/V and where $\alpha_{0,1}$ is the response of the PZT in Hz/V. We write the feedback compensation as

$$G_0(s) = g_{0,0}\big(G_{0,1}(s)A_{0,1} + G_{0,2}(s)A_{0,2}\big) \tag{55}$$

with

$$G_{0,1}(s) = g_{0,1}\frac{1}{1 + {s}/{2\pi f_{0,P6}}}\frac{1}{1 + {s}/{2\pi f_{0,P7}}}\frac{1}{1 + {s}/{2\pi f_{0,P8}}} \tag{56}$$

$$\begin{aligned}
G_{0,2}(s) = g_{0,2}\frac{s + 2\pi f_{0,Z1}}{1 + {s}/{2\pi f_{0,P1}}}\frac{1 + {s}/{2\pi f_{0,Z2}}}{1 + {s}/{2\pi f_{0,P2}}}\frac{1 + {s}/{2\pi f_{0,Z3}}}{1 + {s}/{2\pi f_{0,P3}}} \\
\times \frac{1 + {s}/{2\pi f_{0,Z4}}}{1 + {s}/{2\pi f_{0,P4}}}\frac{1 + {s}/{2\pi f_{0,Z5}}}{1 + {s}/{2\pi f_{0,P5}}}
\end{aligned} \tag{57}$$

The crossover between the PZT path and the Pockels cell path will be around 3 kHz, whereas the unity gain frequency will be near 500 kHz. The actuators and transfer functions of the auxiliary laser are identical and can be deduced from the above equations by replacing each "0" with a "1".

2.2 SHG and OPO length

2.2.1 SHG

For the photodetector to lock the SHG we are using

$$S_4(s) = \eta_4 P_{Main}\eta_{QE,4}\varepsilon_R Z_4 \frac{1}{1 + {s}/{2\pi f_4}} \tag{58}$$

where η_4, P_{Main}, Γ_4, $\eta_{QE,4}$, ε_R, Z_4, and f_4 denote the fractional power on the photodetector, the power of the main laser, the modulation depth, the photodetector quantum efficiency, the

photodetector responsivity in A/W, the photodetector transimpedance gain in Ω, and the pole due to the tuned circuit, respectively. The actuator is a PZT with a response of

$$A_4(s) = \alpha_4 \tag{59}$$

where α_4 is the displacement coefficient in m/V. We write the electronics transfer function $G_4(s)$ as

$$G_4(s) = g_4 \frac{1 + {}^s/_{2\pi f_{4,Z1}}}{1 + {}^s/_{2\pi f_{4,P1}}} \frac{1}{1 + {}^s/_{2\pi f_{4,P2}}} \tag{60}$$

with zeroes and poles at $f_{4,Z1}$, $f_{4,P1}$ and $f_{4,P2}$, respectively. The gain g_4 is adjusted to yield a unity gain frequency of about 1 kHz.

2.2.2 OPO

The OPO feedback is similar to the SHG servo. For the photodetector we write

$$S_5(s) = \eta_5 P_{Main} \eta_{QE,5} \frac{\varepsilon_R}{2} Z_5 \frac{1}{1 + {}^s/_{2\pi f_5}} \tag{61}$$

where η_5, P_{Main}, Γ_5, $\eta_{QE,5}$, ε_G, Z_5, and f_5 denote the fractional power on the photodetector, the power of the main laser, the modulation depth, the photodetector quantum efficiency, the photodetector responsivity in A/W, the photodetector transimpedance gain in Ω, and the pole due to the tuned circuit, respectively. The photodetector responsivity in green is half the one in red. The actuator is a PZT with a response of

$$A_5(s) = \alpha_5 \tag{62}$$

where α_5 is the displacement coefficient in m/V. We write the electronics transfer function $G_5(s)$ as

$$G_5(s) = g_5 \frac{1 + {}^s/_{2\pi f_{5,Z1}}}{1 + {}^s/_{2\pi f_{5,P1}}} \frac{1}{1 + {}^s/_{2\pi f_{5,P2}}} \tag{63}$$

with zeroes and poles at $f_{5,Z1}$, $f_{5,P1}$ and $f_{5,P2}$, respectively. The gain g_5 is adjusted to yield a unity gain frequency of about 1 kHz.

2.3 Coherent Locking

The photodetector for the coherent locking can be described by

$$S_2(s) = 2\eta_2 \eta_{REFL} P_{aux} \eta_{QE,2} \varepsilon_R Z_2 \frac{1}{1 + {}^s/_{2\pi f_2}} \tag{64}$$

with f_2 the bandwidth of the detector, and with

$$\eta_{REFL} = \eta_{REFL,aux} \eta_{REFL,aux2} \tag{65}$$

$$\eta_{REFL,aux} = \left| \frac{r_{OR,2} - r_{OR,1} e^{-2\pi i f_{aux}/f_{O,FSR}}}{e^{-2\pi i f_{aux}/f_{O,FSR}} - r_{OR,1} r_{OR,2}} \right| \approx 1 \tag{66}$$

$$\eta_{REFLS,aux2} = \eta_{OPO}\sqrt{P_{Green}} \frac{r_{OR,2}t_{OR,1}^2}{1 - 2r_{OR,1}r_{OR,2}\cos(2\pi f_{aux}/f_{O,FSR}) + r_{OR,1}^2 r_{OR,2}^2}$$
$$\times \frac{t_{OG,1}}{1 - r_{OG,1}r_{OG,2}} \tag{67}$$

The coherent locking signal is fed back to the additive offset of the auxiliary laser as well as a PZT in the path from the auxiliary laser to the OPO. The PZT and additive offset actuators can be expressed as

$$A_{2,1} = k\alpha_{2,1} \quad \text{and} \quad A_{2,2} = \alpha_{2,2} \tag{68}$$

For a servo compensation filter we use

$$G_2(s) = G_{2,0}(s)\big(G_{2,1}(s)A_{2,1} + G_{2,2}(s)A_{2,2}\big) \tag{69}$$

with

$$G_{2,0}(s) = g_{2,0} \frac{1 + {}^{s}/_{2\pi f_{2,Z1}}}{1 + {}^{s}/_{2\pi f_{2,P1}}} \frac{1 + {}^{s}/_{2\pi f_{2,Z2}}}{1 + {}^{s}/_{2\pi f_{2,P2}}} \frac{1}{1 + {}^{s}/_{2\pi f_{2,P3}}} \tag{70}$$

$$G_{2,1}(s) = g_{2,1} \frac{1}{1 + {}^{s}/_{2\pi f_{2,P4}}} \tag{71}$$

$$G_{2,2}(s) = g_{2,2} \frac{s}{1 + {}^{s}/_{2\pi f_{2,P5}}} \frac{s}{1 + {}^{s}/_{2\pi f_{2,P6}}} \tag{72}$$

Adjusting the gain in the PZT path we can set the crossover frequency around a few kHz. The overall gain determines the bandwidth of the servo and can be set as high as about 100 kHz. This is limited by the bandwidth of the laser locking servos since we are running out of actuator gain near its unity gain frequency. The additive offset path is AC-coupled to limit the amount of low frequency feedback range needed in this path. The overall open loop transfer function has two boost stages to increase low frequency suppression.

2.4 Local Oscillator

The photodetector for the local oscillator locking can be described by

$$S_3(s) = 2\sqrt{\eta_{Aux,3}\big(\eta_{TRANS,aux} + \eta_{TRANS,aux2}\big)P_{Aux}\eta_{LO,3}P_{LO}\eta_{QE,3}\varepsilon_R Z_3} \frac{1}{1 + {}^{s}/_{2\pi f_3}} \tag{73}$$

with f_3 the bandwidth of the detector, and with

$$\eta_{TRANS,aux} = \left|\frac{t_{OR,1}t_{OR,2}}{e^{2\pi i f_{aux}/f_{O,FSR}} - r_1 r_2}\right| \tag{74}$$

$$\eta_{TRANS,aux2} = \eta_{OPO}\sqrt{P_{Green}} \frac{t_{OR,1}t_{OR,2}}{1 - 2r_{OR,1}r_{OR,2}\cos(2\pi f_{aux}/f_{O,FSR}) + r_{OR,1}^2 r_{OR,2}^2}$$
$$\times \frac{t_{OG,1}}{1 - r_{OG,1}r_{OG,2}} \tag{75}$$

The field amplitude asymmetry the becomes

$$\alpha = \frac{\eta_{TRANS,aux} - \eta_{TRANS,aux2}}{\eta_{TRANS,aux} + \eta_{TRANS,aux2}} \tag{76}$$

The local oscillator locking signal is fed back to the additive offset of the main laser as well as a PZT in the path of the green light. Alternatively, the PZT can be placed in the fiber path, or altogether eliminated by feeding back to a VCO which feeds an AOM in the fiber path.

The PZT and additive offset actuators can be expressed as

$$A_{3,1} = k\alpha_{3,1} \quad \text{and} \quad A_{3,2} = \alpha_{3,2} \tag{77}$$

For a servo compensation filter is identical to the one used for the coherent locking

$$G_3(s) = G_{3,0}(s)\big(G_{3,1}(s)A_{3,1} + G_{3,2}(s)A_{3,2}\big) \tag{78}$$

with

$$G_{3,0}(s) = g_{3,0} \frac{1 + {}^s\!/_{2\pi f_{3,Z1}}}{1 + {}^s\!/_{2\pi f_{3,P1}}} \frac{1 + {}^s\!/_{2\pi f_{3,Z2}}}{1 + {}^s\!/_{2\pi f_{3,P2}}} \frac{1}{1 + {}^s\!/_{2\pi f_{3,P3}}} \tag{79}$$

$$G_{3,1}(s) = g_{3,1} \frac{1}{1 + {}^s\!/_{2\pi f_{3,P4}}} \tag{80}$$

$$G_{3,2}(s) = g_{3,2} \frac{s}{1 + {}^s\!/_{2\pi f_{3,P5}}} \frac{s}{1 + {}^s\!/_{2\pi f_{3,P6}}} \tag{81}$$

Adjusting the gain in the PZT path we can set the crossover frequency around a few kHz. The overall gain determines the bandwidth of the servo and can be set as high as about 100 kHz. This is limited by the bandwidth of the laser locking servos since we are running out of actuator gain near its unity gain frequency. The additive offset path is AC-coupled to limit the amount of low frequency feedback range needed in this path. The overall open loop transfer function has two boost stages to increase low frequency suppression.

Since the local oscillator servo effectively locks the main laser to the PSL through the DC offset field at the antisymmetric port, one might wonder if the laser locking of the main laser to the PSL through a fiber is still necessary. In principle, one could eliminate the laser locking loop, but in practice the main laser and the PSL have to be within a few 10s of kHz to make this work. Locking the main laser to the PSL through a fiber first will guarantee that the laser runs at the correct frequency. The local oscillator network then only needs to lock the phase. Feeding back using an additive offset to the main laser also has the advantage to greatly increase the bandwidth and the low frequency suppression. This almost certainly will make a fiber stabilization system unnecessary.

3 Noise Couplings and Requirements

3.1 Acoustic Couplings

3.1.1 Back Scattering

Back scattering has been calculated for the output mode cleaner (OMC) in T060303-v1. We are following the same derivation. Using Eqn. (3) of the above paper, we require

$$x_{SC}\sqrt{R_r} < 10^{-17} \text{ m/}\sqrt{\text{Hz}}, \quad f > 10 \text{ Hz}, \tag{82}$$

where x_{SC} is the motion of the scattering surface along the direction of the beam propagation vector and R_r is the power reflectivity, into the interferometer TEM00 mode, of the scattering surface.

We assume that the fraction of light at the AS port deflected into the squeezer path by the thin-film polarizer is 10^{-3}, and that the rejection of the in-vacuum Faraday isolator in the squeezer path is 10^{-3} as well. Any light reflected back into the squeezer path will then go straight back into the interferometer. Looking first at the output window on HAM4 and taking the reflectivity value from Table 1 in T060303, we get

$$\sqrt{R_r} \approx 3 \times 10^{-12} \quad \text{and} \quad x_{SC} < 4 \times 10^{-6}. \tag{83}$$

Looking at Figure 4 in T060303 we can see that this is easily fulfilled.

Once on the squeezer breadboard the largest back scattering is due to the OPO itself. Since the OMC and the OPO are very similarly constructed cavities, we assume their reflectivities will be similar too. The OMC reflectivity[1] is estimated to be 6×10^{-10}, whereas high quality steering optics will be in the range from 2×10^{-13} (0.7 mm beam waist) to 6×10^{-14} (4.5 mm beam waist).

Figure 2 shows a typical spectrum of the motion of an optical table in the LVEA. We are approximating the spectra with

$$x_{SC} \approx \begin{cases} \dfrac{10^{-6}}{f^2} \text{ m} \cdot \text{Hz}^{3/2} & \text{for an optics table straight on the floor,} \\ \dfrac{10^{-8}}{f^2} \text{ m} \cdot \text{Hz}^{3/2} & \text{for an accoustically isolated table.} \end{cases} \tag{84}$$

Substituting back into the requirement and including the factor 10^{-6} from the thin-film polarizer and the in-vacuum Faraday isolator, we get a requirement on the overall back-scattering reflectivity coefficient of the squeezer setup

$$\sqrt{R_{SQZ}} \approx \begin{cases} 10^{-4} \left(\dfrac{f}{100 \text{ Hz}}\right)^2 & \text{for an optics table straight on the floor,} \\ 10^{-2} \left(\dfrac{f}{100 \text{ Hz}}\right)^2 & \text{for an accoustically isolated table.} \end{cases} \tag{85}$$

---

[1] The combined reflectivity of the OMC and the Faraday isolator has been measured to be $\sqrt{R_r} = 3 \times 10^{-8}$ (see LLO ilog from 1/28/2009, and corrected for the 50/50 beam splitter which was installed during the measurement).

For the H1 squeezer experiment we set $f = 100\,\text{Hz}$ and use the first requirement. This sets the requirement for $R_{SQZ} < 10^{-8}$. The estimate for the OPO reflectivity is well below that and so are all the steering optics.

For advanced LIGO the lowest frequency of interest is 10 Hz. This will require the placement of the squeezer table into an acoustically isolated enclosure. Special care needs to be taken to avoid increasing the acoustically induced path fluctuations by introducing large resonances in the optical components on the squeezer table.
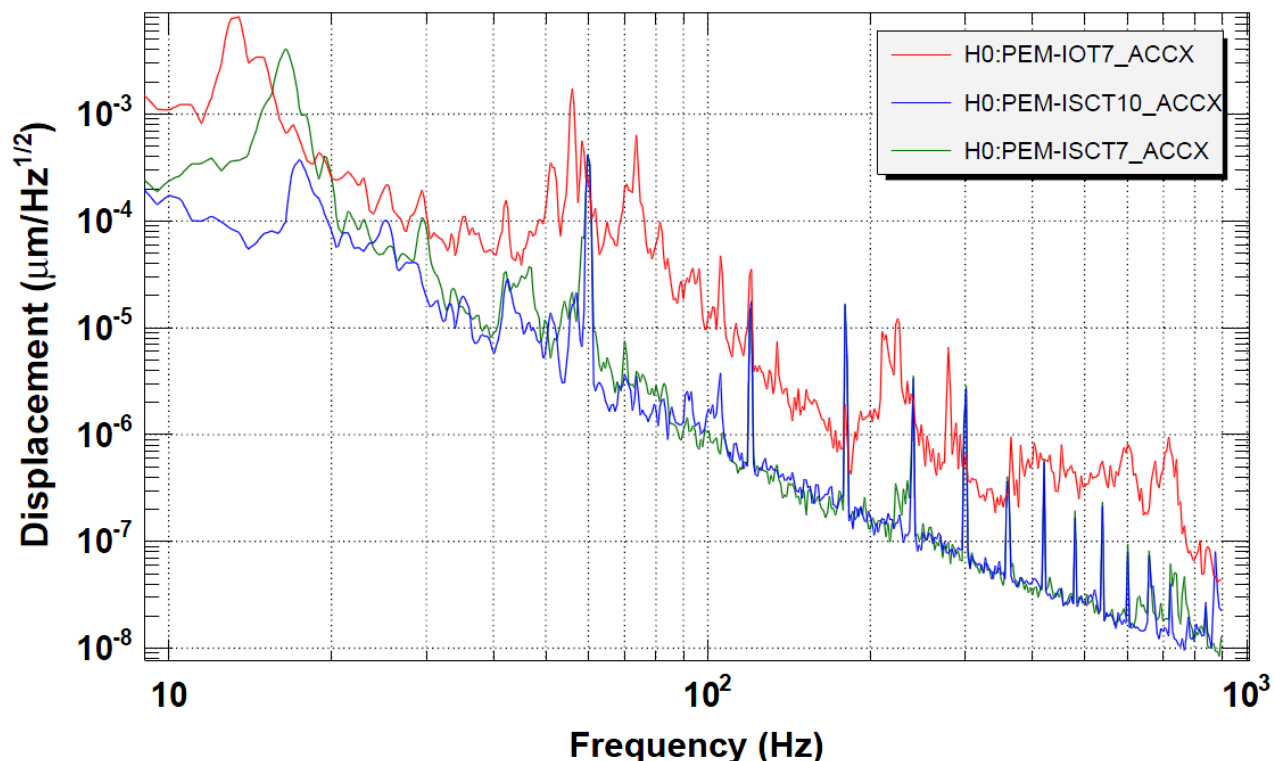
Figure 2: Motion of an optics table in the LVEA. IOT7 and ISCT7 are standard optics table with fixed legs resting on the ground. ISCT7 and ISCT10 are located inside an acoustic enclosure. Above 100 Hz the displacement spectra for ISCT7 and 10 are limited by the noise of the accelerometers.

3.1.2 Beam Jitter

Beam jitter and static misalignment can reduce the power coupled through the output mode cleaner. This will look like a straight power loss and can be added to the power budget. To get a 10% loss in transmitted power the static misalignment needs to be as large as a third of the divergence angle. Static misalignment will be smaller than this—certainly, if an auto-alignment system is used.

Beam jitter can also couple with a static misalignment to generate a longitudinal phase shift. We write

$$\Delta\varphi \approx \frac{\alpha_0\,\Delta\alpha}{2} \tag{86}$$

17

These fluctuations will be suppressed by both the local oscillator feedback servo and a possible auto-alignment system. Hence, they are unlikely a significant contribution to the error budget.

3.2 Squeezed Beam Requirements

3.2.1 Squeezer Level

We require 3 dB of squeezing at the interferometer antisymmetric port. To allow for significant optical losses in the injection path and the interferometer we require the squeezer itself to demonstrate 6 dB of squeezing.

3.2.2 Phase Noise

If the squeezer produces a squeezed state of 6 dB and 14 dB of anti-squeezing, the expected squeezed state after 25% of additional optical losses in the interferometer is 3.5 dB. This corresponds to a combined total optical loss of about 40%. Figure 3 shows that with 60% propagation efficiency 3.3 degrees of phase fluctuations will degrade the squeezed state to about 3 dB. We therefore set a requirement on the total phase noise of the squeezed vacuum state relative to the DC locking field at the antisymmetric port of 50 mrad rms.
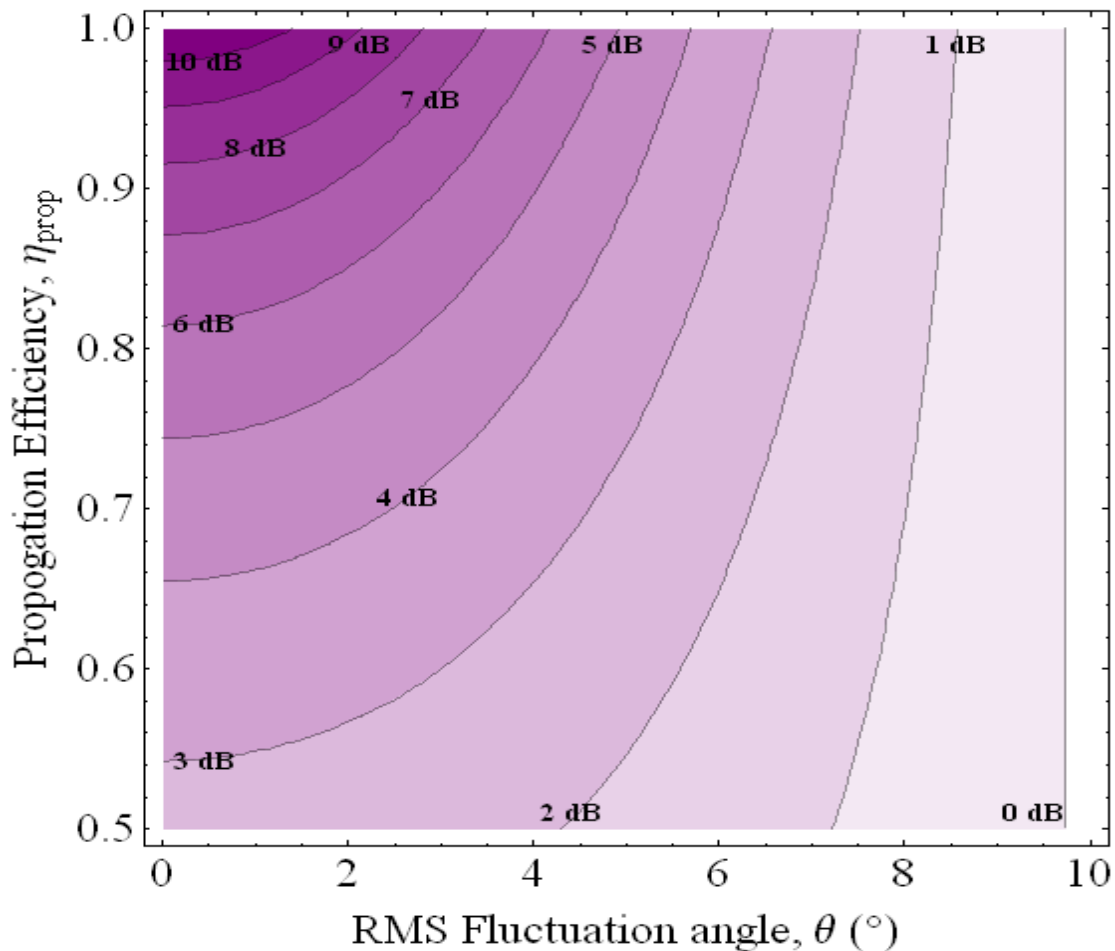

Figure 3: Expected squeezing level from 0 dB to 10 dB as function of the propagation efficiency and the RMS fluctuation angle.

3.3 Losses

The relevant optical losses from the squeezer output into the interferometer and out onto the photodetector at the antisymmetric port are shown in Table 1.

Table 1: Optical losses from the squeezer to the antisymmetric port photodetector.

Component	Transmission	Uncertainty	Reference
Vacuum window	0.998	0.002	
1st Faraday isolator	0.95	0.02	
2nd Faraday isolator (side injection)	0.95	0.02	
Reflection Michelson/arm cavities	0.98	0.01	
2nd Faraday isolator (through)	0.94	0.02	[2]
Septum window	0. 998	0.2	[3]
OMC mode matching	0. 74	0.002	
OMC cavity losses	0.967	0.005	[4]
DC photodetector QE	0.98	0.01	[5]
Total	**0.745**	**0.043**	

3.4 Modulation Sidebands

The RF modulation sidebands are large at the antisymmetric port. They will be rejected by the output mode cleaner which has a power transmission coefficient of $T_{SB}=0.9\%$ at 25 MHz offset. The free-spectral-range is 287 MHz and the input and output coupler have a 8000 ppm transmission. With 8 W power into the H1 interferometer about 10 mW carrier light gets passed through the output mode cleaner. About 0.4 mW of this light is due to contrast defect whereas the remainder is due to the length offset. A scan of the OMC length revealed that the RF sideband power in the OMC mode is about the same for each sideband as for the carrier[6]. The phase noise contribution has 2 terms: a term due to the sidebands beating against the carrier in the contrast defect and a term due to the imbalance of the sidebands.

---

[2] LHO ilog from 8/4/2008

[3] LHO ilog from 8/12/2008

[4] LHO ilog from 8/4/2008

[5] LHO ilog from 8/1/2008

[6] LHO ilog from 7/8/2009

If we write

$$P_{CD} = \frac{P_{CR}}{\eta} \tag{87}$$

with P_{CD} the power due to the contrast defect and P_{CR} the total carrier power after the OMC. For the sidebands we can write
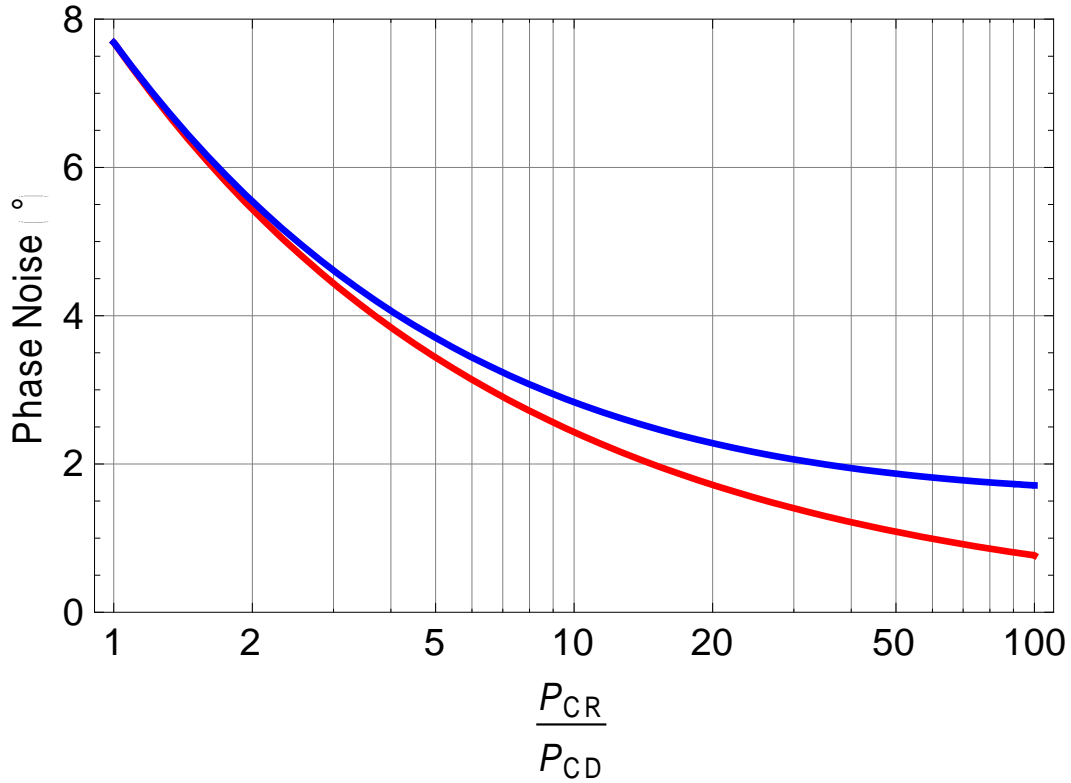
$$P_{SB} = P_{SB+} + P_{SB-} \tag{88}$$

$$\Delta P_{SB} = P_{SB+} - P_{SB-} = 2\varepsilon\, P_{SB} \tag{89}$$

The rms phase fluctuations then becomes

$$\Gamma_{rms} = \sqrt{T_{SB} \frac{P_{SB}}{P_{CR}}\left(\frac{1}{\eta} + \varepsilon^2 \frac{\eta - 1}{\eta}\right)} \tag{90}$$

Figure 4 shows the phase noise due to the RF sidebands as function of η. The current value for η at the H1 interferometer is around 25 which yields a rms phase noise of about 1.5° which corresponds to about 25 mrad and is below the requirement.


Figure 4: Phase noise due to the RF sidebands at the AS port after the OMC. The curve is given as a function of the ratio of the total carrier power over the carrier power due to contrast defect. The red curve is for $\varepsilon = 0$, whereas the blue curve is for a very large $\epsilon = 0.2$.

3.5 Noise Couplings

Using the servo model from the previous section we are looking at the noise couplings into the phase angle of the squeezed field. Using worst case spectra we can then propagate the corresponding noise terms into phase fluctuations of the squeezed field. We have established a requirement on the phase fluctuations of the squeezed field of 50 mrad rms. We translate this into a requirement on each of the technical noise terms of no more than 5 mrad rms. All calculations in this section are made with an auxiliary laser field asymmetry of $\alpha = 0.33$.

3.5.1 Laser Noise

We include frequency noise from the PSL, the main laser and the auxiliary laser, as well as intensity noise from the main and auxiliary laser. Figure 5 shows the magnitude transfer functions for these couplings. Due to our high bandwidth feedback compensation networks laser frequency noise is greatly suppressed. The coupling of laser intensity noise is intrinsically small, since its only direct coupling is due to the coherent field which is passed through the OPO off-resonance.
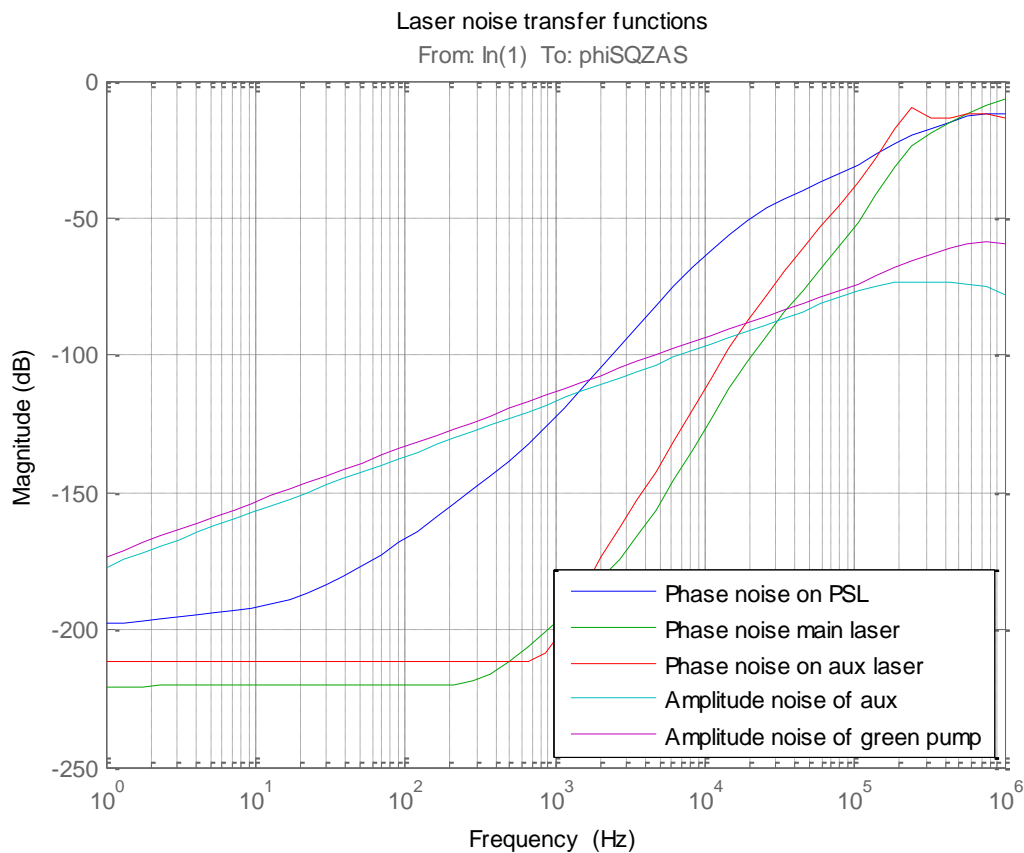
Figure 5: Transfer functions of laser noise into the squeezer phase noise.

21

We take the free running laser frequency noise from Figure 5 in T990025-00 and approximate a worst case spectrum with the following equation

$$N_{\Delta f}^{free}(f) = \begin{cases} 200 \; \frac{\text{Hz}}{\sqrt{\text{Hz}}} & \text{for } f \leq 100 \text{ Hz} \\ 200 \; \frac{\text{Hz}}{\sqrt{\text{Hz}}} \times \frac{100 \text{ Hz}}{f} & \text{for } f > 100 \text{ Hz} \end{cases} \tag{91}$$

The stabilized laser frequency noise is used for the PSL and is taken from Figure 3 in T000031-00. We use

$$N_{\Delta f}^{stab}(f) = \begin{cases} 0.02 \; \frac{\text{Hz}}{\sqrt{\text{Hz}}} & \text{for } f \leq 1 \text{ MHz} \\ 0.02 \; \frac{\text{Hz}}{\sqrt{\text{Hz}}} \times \frac{1 \text{ MHz}}{f} & \text{for } f > 1 \text{ MHz} \end{cases} \tag{92}$$
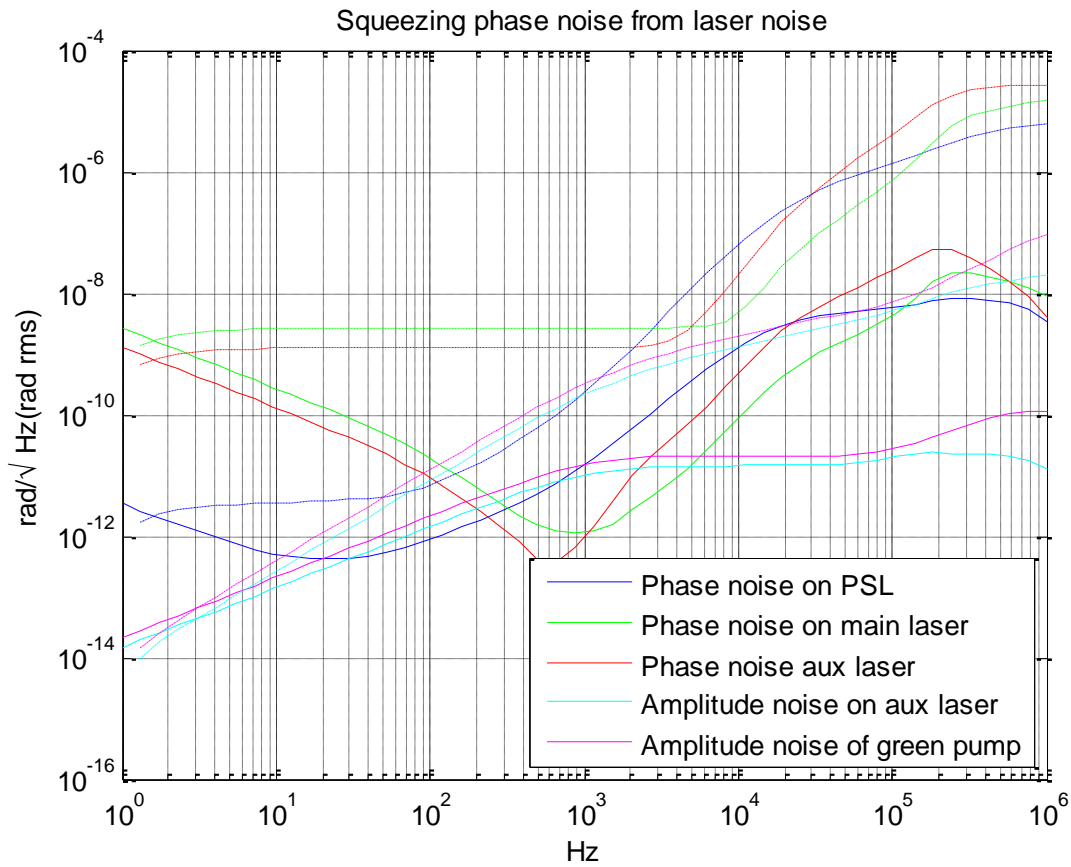
Figure 6: Squeezer phase noise due to laser noise.

The free running intensity noise is taken from Figure 6 in T990025-00. We are limiting the high frequency roll-off to the level of shot noise at 1 mW—again, a worst case assumption. We use the following equation for the relative intensity noise

$$N_{\Delta A}^{free}(f) = \begin{cases} 10^{-5} \big/ \sqrt{\text{Hz}} & \text{for } f \le 1 \text{ kHz} \\ 10^{-5} \big/ \sqrt{\text{Hz}} \times \dfrac{1 \text{ kHz}}{f} & \text{for } f > 1 \text{ kHz} \text{ and } f \le 100 \text{ kHz} \\ 10^{-7} \big/ \sqrt{\text{Hz}} & \text{for } f > 100 \text{ kHz} \end{cases} \qquad (93)$$

Figure 6 shows these noise sources propagated to the phase angle of the squeezed field. The requirement on the rms phase noise is easily met.

3.5.2 Path Length Fluctuations

We investigate path length fluctuations in the input path due to fiber noise. Path length fluctuations on the laser table itself due to flexing of the optical table or the non-rigidity of optical mounts are added to the main laser beam path, to path of the auxiliary laser, to the path of the green light and to the path towards the interferometer. Figure 7 shows the magnitude transfer functions for these couplings. Again, these fluctuations are greatly suppressed due to our servos.
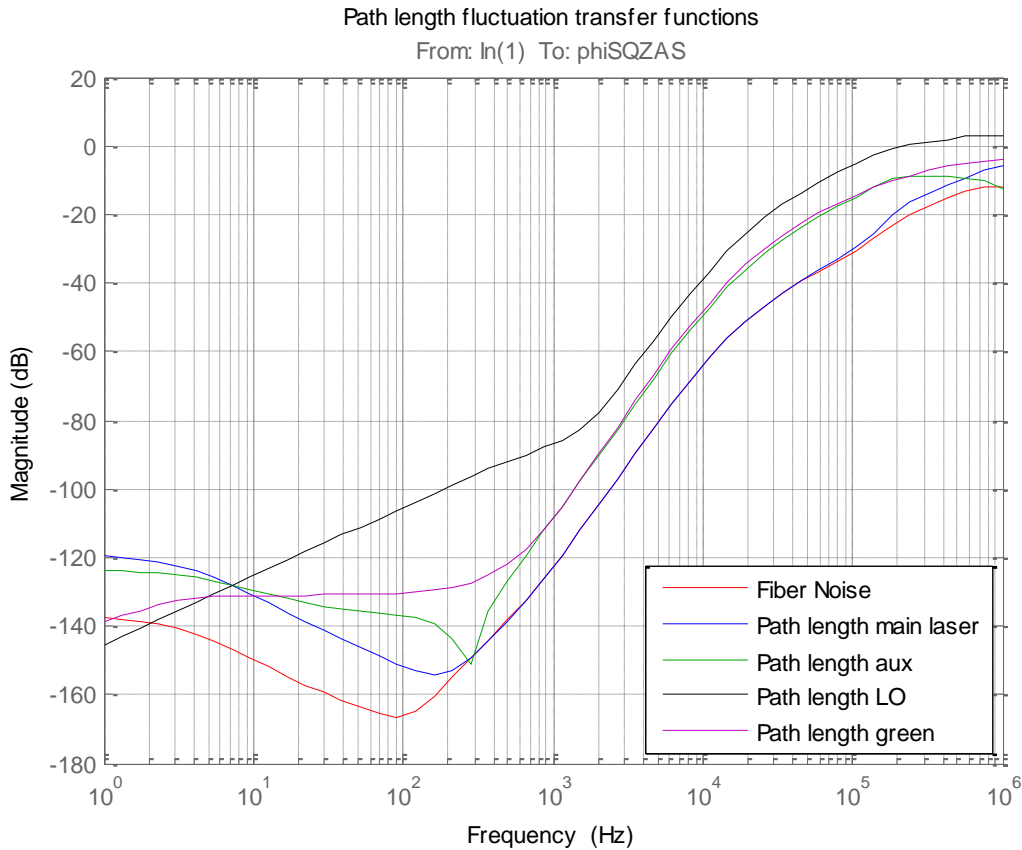

Figure 7: Transfer functions of path length fluctuations into squeezer phase noise.

For the input to the path length fluctuations we are using Figure 2Figure 2: Motion of an optics table in the LVEA. IOT7 and ISCT7 are standard optics table with fixed legs resting on the ground. ISCT7 and ISCT10 are located inside an acoustic enclosure. Above 100 Hz the displacement spectra for ISCT7 and 10 are limited by the noise of the accelerometers., and approximate with

$$N_{\Delta x}(f) = 10^{-10}\,{}^{m}\!/_{\sqrt{\text{Hz}}} \times \left(\frac{100\,\text{Hz}}{f}\right)^{2} \tag{94}$$

Fiber noise was measured in Figure 2 of T0900376-v1. It is no worse than the free running frequency noise of a laser and we can just use its spectra.

Multiplying the noise spectra with the transfer functions we get the curves in Figure 8. Again, the requirement on the rms phase noise of the squeezed field is met easily.
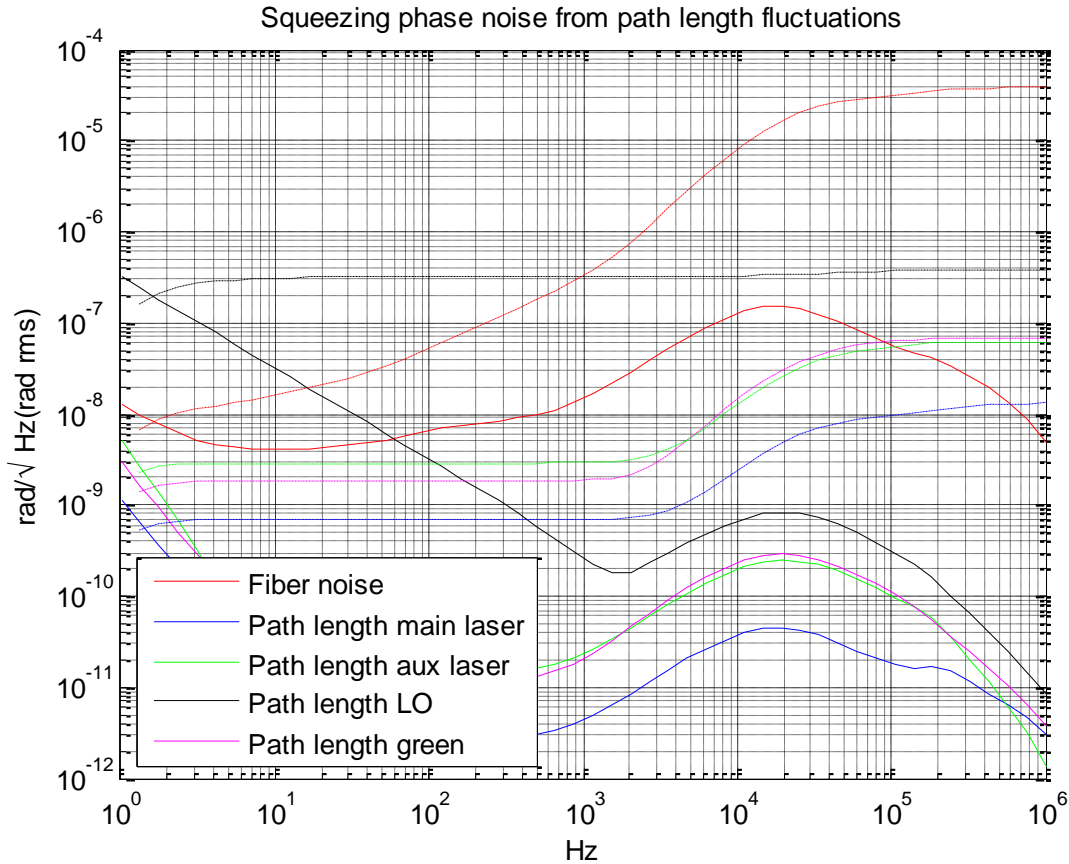
Figure 8: Squeezer phase noise due to path length variations.

3.5.3 Displacement Noise

Displacement noise couplings of both the SHG and the OPO cavity length are shown in Figure 9. There is a significant difference between the two: the displacement noise of the SHG is suppressed by the local oscillator feedback, whereas the one of the OPO is not. Displacement noise will affect the coherent fields at the antisymmetric port differently from the squeezed field. Therefore zeroing the effect on the local oscillator error signal will not suppress the effect on the squeezed field. On

the other hand displacement noise of the SHG will add phase noise to the green light which then can be suppressed with the local oscillator servo.

We use the same length fluctuations as in the equation above. These are the length fluctuations as measured on the top of an optical table and therefore will overestimate the relative displacement noise of a rigid structure. Even with these assumptions we still meet the requirement. The curves are presented in Figure 10.
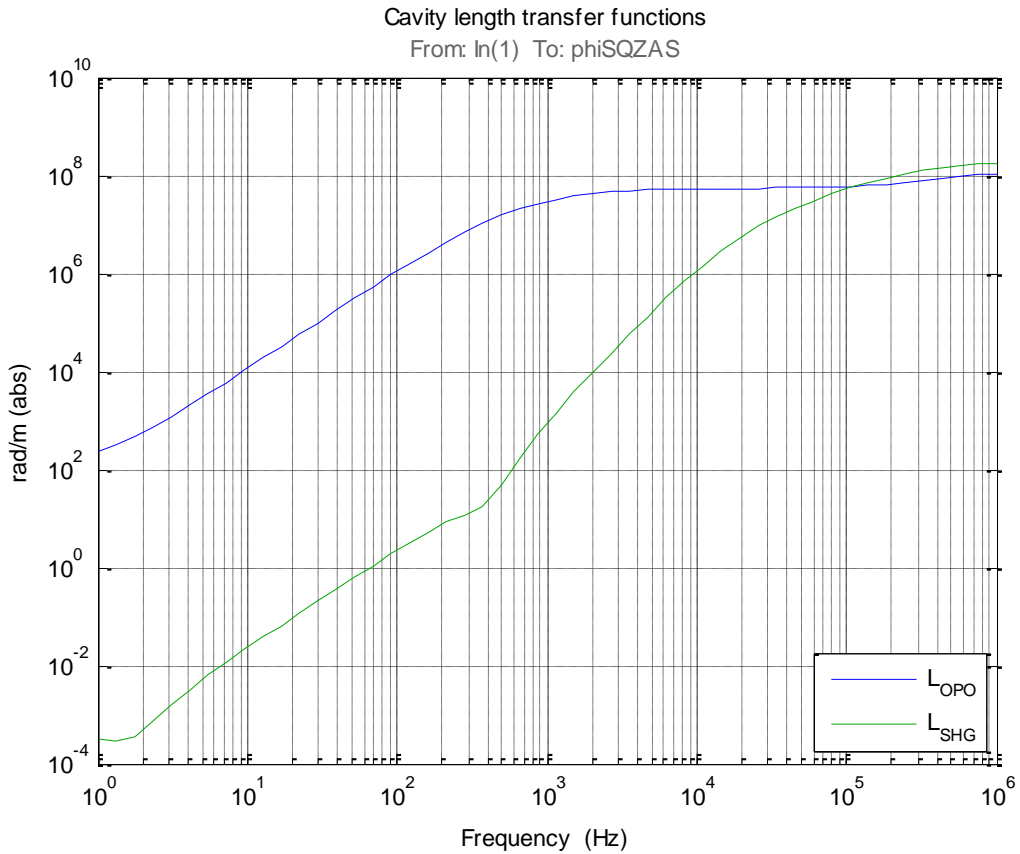
Figure 9: Transfer functions of cavity displacement noise into squeezer phase noise.

Squeezing phase noise from cavity length fluctuations
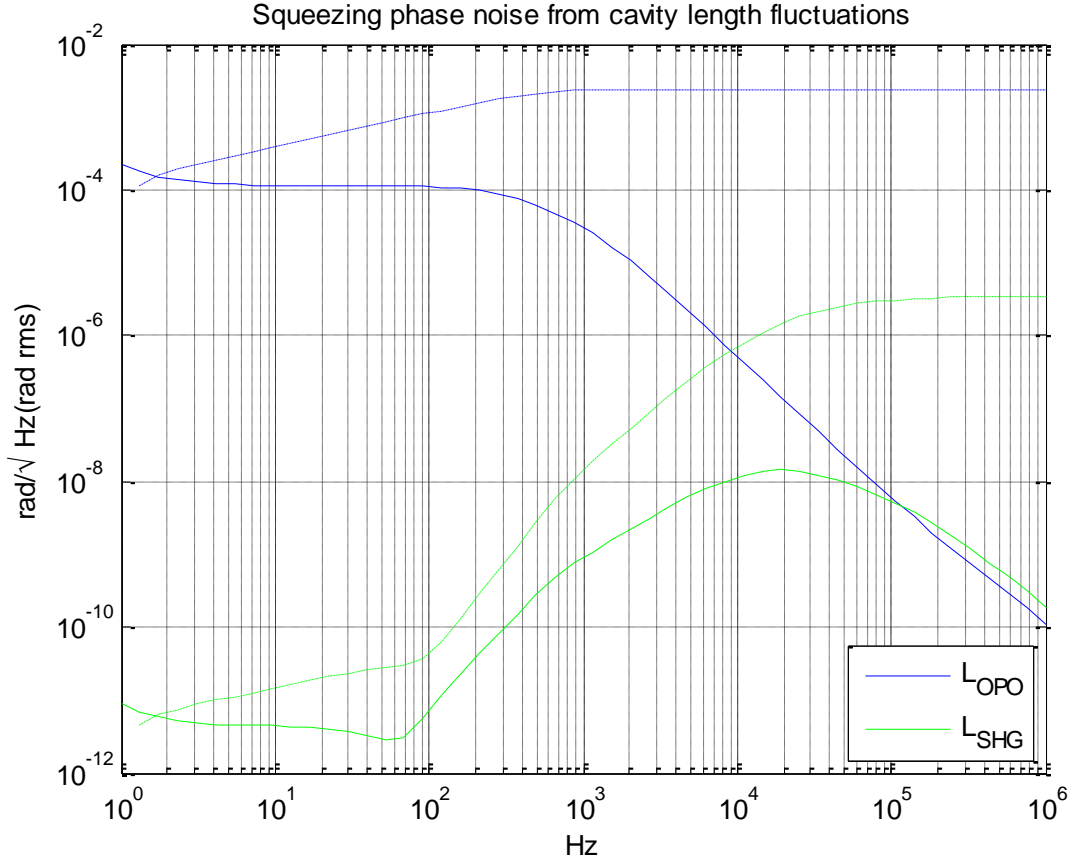
Figure 10: Squeezer phase noise due to cavity displacement noise.

3.5.4 Shot Noise

Shot noise at the output of the nth photodetector can be written as

$$N_n^{shot}(f) = \sqrt{2q\, \eta_{QE,n}\varepsilon_R P_n}\; Z_n \begin{cases} 1 & \text{for } n = 0, 1 \\[2mm] \dfrac{1}{1 + {}^{s}/_{2\pi f_n}} & \text{for } n = 2, 3, 4 \\[2mm] \dfrac{1}{\sqrt{2}}\dfrac{1}{1 + {}^{s}/_{2\pi f_n}} & \text{for } n = 5 \end{cases} \qquad (95)$$

where $q = 1.602176487(40) \times 10^{-19}$ is the elementary charge, P_n denotes the total light power incident on the photodetector, $\eta_{QE,n}$ denotes the quantum efficiency, ε_R denotes the photodetector responsivity in A/W, Z_n denotes the photodetector transimpedance gain in Ω, and f_n denotes the pole due to the tuned circuit, respectively. Photodetector 5 measures green light and we include a factor of $1/\sqrt{2}$ for the reduction of the photodetector responsivity.

For the incident power on each detector we estimate

$$
\begin{array}{lcr}
P_0 & \eta_{PSL,0}P_{PSL} + \eta_{Main,0}P_{Main} & 1.5 \text{ mW} \\[6pt]
P_1 & \eta_{Main,1}P_{Main} + \eta_{Aux,1}P_{Aux} & 1.5 \text{ mW} \\[6pt]
P_2 & \eta_2\eta_{REFL,aux}P_{Aux} & 0.5 \text{ mW} \\[6pt]
P_3 & \eta_{LO,3}(P_{LO} + P_{CD}) & 1.0 \text{ mW} \\[6pt]
P_4 & \eta_4|t_{SR,CR}|^2 P_{Main} & 1.3 \text{ mW} \\[6pt]
P_5 & \eta_5 P_{Main} & 1.0 \text{ mW}
\end{array}
\tag{96}
$$

where we neglect the power in f_{Aux2} on photodetector 2 and where we neglected the power in f_{Aux} and f_{Aux2} on photodetector 3. P_{CD} denotes the power in all other modes other an TEM00 of the carrier local oscillator field. It includes higher order modes as well as the RF sidebands. In reality, P_{CD} may be ten times larger than P_{LO}.
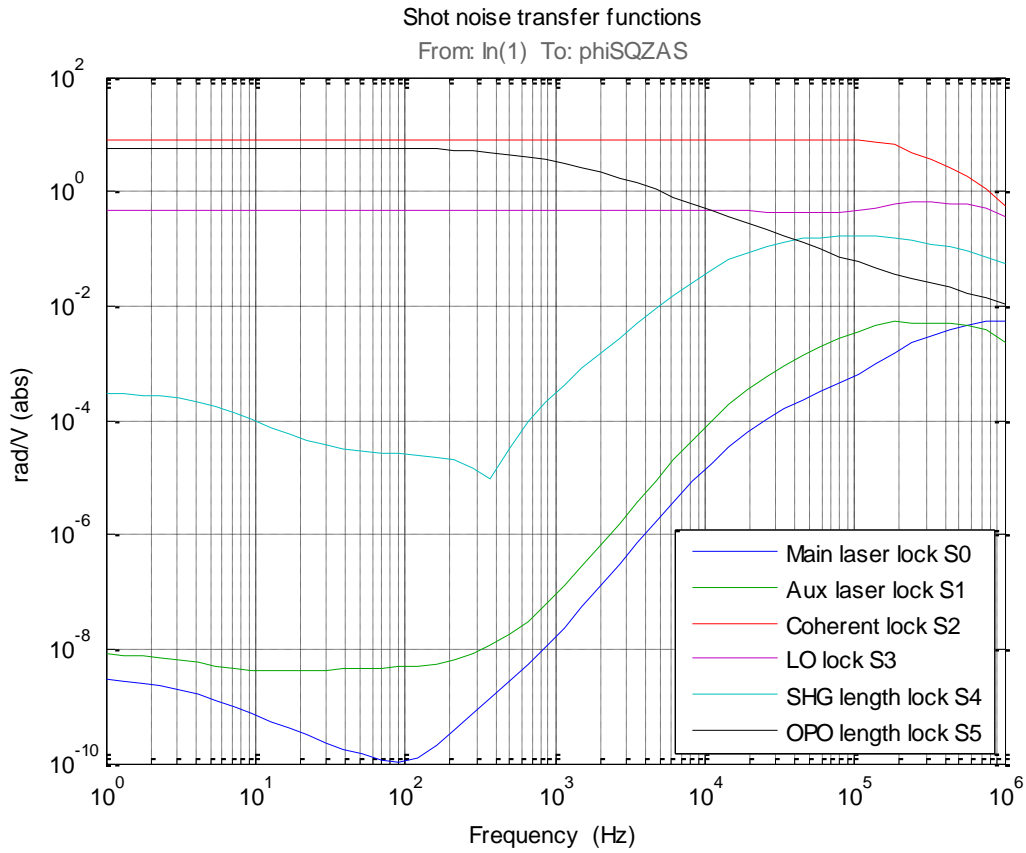
Figure 11: Transfer functions of shot noise contributions into squeezer phase angle.

Figure 11 shows the magnitude transfer functions for coupling shot noise into squeezer phase angle. The most critical coupling is due to shot noise in the coherent locking. This is mostly due to the fact the signal is rather small in reflection of the OPO and hence on photodetector S_2. Figure 12 shows the resulting squeezer phase noise when we add the shot noise from the above power estimations. The resulting rms noise levels are well below our requirement.
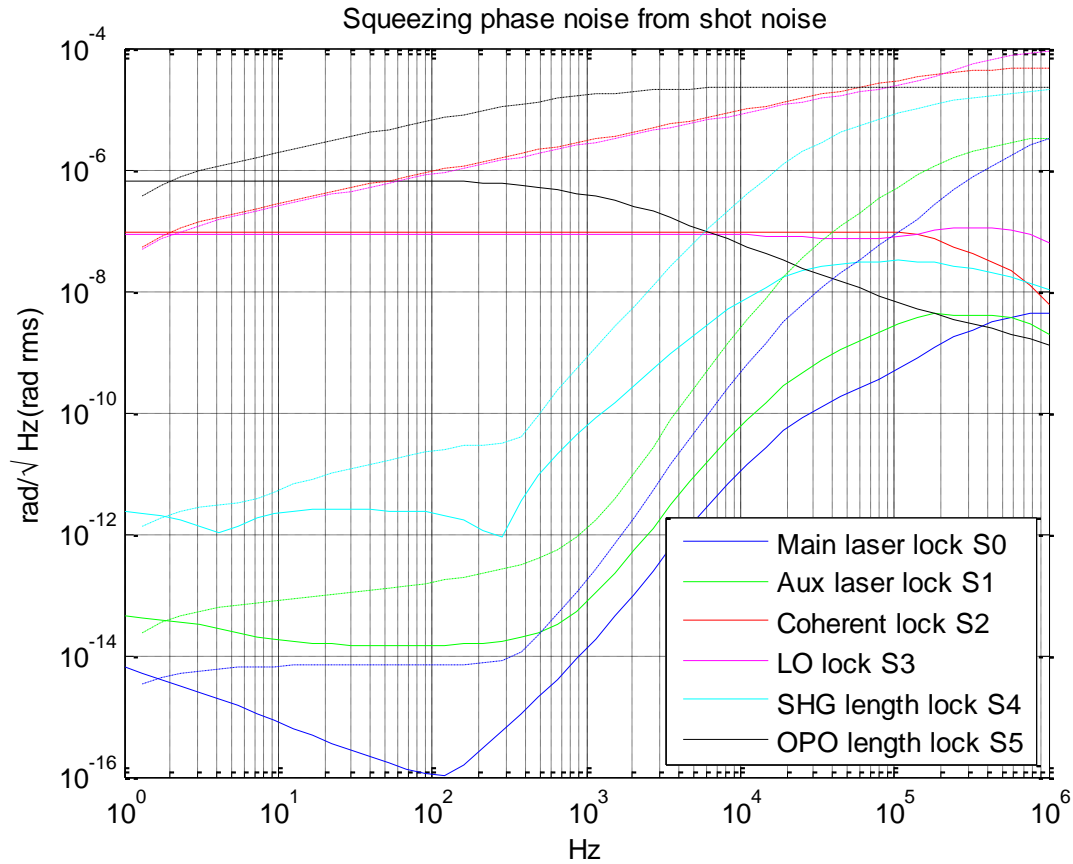
Figure 12: Squeezer phase noise due to shot noise on the photodetectors.

4 Fabry-Perot Resonators

4.1 Cavity Parameters

4.1.1 SHG

The SHG cavity is a linear configuration. Parameters are listed in Table 2.

Table 2: Optical parameters for the SHG cavity.

Parameter	Description	Value	Unit
L_S	Physical length	47.35	mm
l_S	Effective length (10 mm PPKTP)	54.75	mm
$f_{S,FSR}$	Free-spectral-range	2.7	GHz
λ_R	Red wavelength	1064	nm
λ_G	Green wavelength	531	nm
$r_{SG,1}^2$	Green input mirror reflectivity	0.01	
$r_{SG,2}^2$	Green output mirror reflectivity	1.0	
$r_{SR,1}^2$	Red input mirror reflectivity	0.9	
$r_{SR,2}^2$	Red output mirror reflectivity	0.9992	
δ_{SR}	Red power loss (conversion coeff.)	0.05	
F_{SG}	Green Finesse	1.1	
F_{SR}	Red Finesse	39.9	
f_{SR}	Red cavity pole	34.3	MHz
$f_{S,M}$	Modulation frequency	35.5	MHz
$\Gamma_{S,M}$	Modulation depth	0.01	

4.1.2 OPO

The OPO cavity is a bowtie configuration. Parameters are listed in Table 3.

Table 3: Optical parameters for the OPO cavity.

Parameter	Parameter	Value	Unit
l_O	Half length	0.14	m
$f_{O,FSR}$	Free-spectral-range	1.071	GHz
$r_{OG,1}^2$	Green input mirror reflectivity	0.7	

$r_{OG,2}^2$	Green output mirror reflectivity	1.0	
$r_{OR,1}^2$	Red input mirror reflectivity	0.99	
$r_{OR,2}^2$	Red output mirror reflectivity	0.85	
F_{OG}	Green Finesse	17.6	
F_{OR}	Red Finesse	36.4	
f_{OG}	Green cavity pole	30.4	MHz
f_{OR}	Red cavity pole	14.7	MHz
$f_{O,M}$	Modulation frequency	71	MHz
$\Gamma_{O,M}$	Modulation depth	0.01	
$\eta_{OPO}\sqrt{P_{Green}}$	Conversion factor for coherent field	0.0276	

4.1.3 Interferometer

Some relevant parameters of the LIGO interferometer are listed in Table 4.

Table 4: Optical parameters for the interferometer.

Parameter	Parameter	Value	Unit
f_{MC}	Mode cleaner pole	4	kHz
f_{IFO}	Double cavity pole	2	Hz

4.2 Cavity Equations

4.2.1 Pound-Drever-Hall Signals

Assuming the RF sidebands are well outside the cavity resonance and omitting the factor $J_0(\Gamma)J_1(\Gamma)P$ which describes the power and modulation depth of the incident beam, the cavity transfer function of a Pound-Drever-Hall reflection locking signal can be written as:

$$T_{REFL}^{\delta l}(s) = -\frac{4Fk}{\pi}\frac{1-r_1^2}{1-r_1 r_2}\sqrt{r_1 r_2}\frac{1}{1+s/\omega_{cav}} \tag{97}$$

with F the cavity finesse, r_1 and r_2 the amplitude reflection coefficients of the input and output mirror, respectively, and ω_{cav} the cavity pole angular frequency:

$$F = \frac{\pi\sqrt{r_1 r_2}}{1-r_1 r_2} \tag{98}$$

$$\omega_{cav} = \pi\frac{f_{FSR}}{F} \tag{99}$$

and $f_{FSR} = c/2L$ the free-spectral-range of the cavity. A similar equation can be written for phase fluctuations injected into the cavity:

$$T_{REFL}^{\phi}(s) = -4F \frac{1 - r_1^2}{1 - r_1 r_2} \sqrt{r_1 r_2} \frac{s}{\omega_{FSR}} \tag{100}$$

The equations for an error signal in transmission are practically the same, but have to include a factor from the sideband transmission amplitude.

$$T_{TRANS}^{\delta l}(s) = -\frac{4Fk}{\pi} |t_{SB}| \frac{\sqrt{1 - r_1^2}\sqrt{1 - r_2^2}}{1 - r_1 r_2} \sqrt{r_1 r_2} \frac{1}{1 + s/\omega_{cav}} \tag{101}$$

$$t_{SB} = \frac{\sqrt{1 - r_1^2}\sqrt{1 - r_2^2}}{1 - e^{2\pi i f_M / f_{FSR}} r_1 r_2} \tag{102}$$

with f_M the modulation frequency. Again, we neglect contributions from the RF sidebands which are small as long as $f_M \gg f_{cav}$. And for the laser phase noise:

$$T_{TRANS}^{\phi}(s) = -4F|t_{SB}| \frac{\sqrt{1 - r_1^2}\sqrt{1 - r_2^2}}{1 - r_1 r_2} \sqrt{r_1 r_2} \frac{s}{\omega_{FSR}} \tag{103}$$

For situations where the modulation frequency is close to the cavity pole one will experience an additional loss of signal. One might be tempted to estimate this factor with

$$T_{loss} \sim \left| \frac{i f_M}{f_{cav} + i f_M} \right| \tag{104}$$

However, this can be quiet inaccurate for $f_M \lesssim f_{cav}$, especially, in reflection when the rear mirror is a high reflector.

4.2.2 Electric Fields

We are looking at an electric field entering a cavity. An off-resonant field can be characterized by its frequency shift away from resonance by a phase angle

$$\varphi = \frac{2\pi f}{f_{FSR}} \tag{105}$$

The field inside the cavity can always be decomposed into a phase-modulated and an amplitude-modulated component, Γ_{CAV} and ΔA_{CAV}, respectively. If we make the ansatz that the input beam has a phase modulation Γ and a relative amplitude modulation ΔA, and if we denote a small length variation by δl, the components inside the cavity can be written as

$$\Gamma_{CAV} = \gamma_{\delta l}(\varphi) H_1(s, \varphi) \delta l + H_2(s, \varphi)\Gamma + \gamma_{\Delta A}(\varphi) \frac{s}{f_{FSR}} H_3(s, \varphi)\Delta A \tag{106}$$

$$\Delta A_{CAV} = \alpha_{\delta l}(\varphi) H_3(s, \varphi) \delta l + \alpha_{\Gamma}(\varphi) \frac{s}{f_{FSR}} H_3(s, \varphi)\Gamma + H_2(s, \varphi)\Delta A \tag{107}$$

For the fields propagating back to the input mirror the carrier field is

$$E_{CAV}^{cr} = \frac{t_1 r_2}{e^{i\varphi} - r_1 r_2} E_{IN}^{cr} \tag{108}$$

and the coefficients become

$$\gamma_{\delta l}(\varphi) = -2k \frac{1 - r_1 r_2 \cos\varphi}{1 - 2r_1 r_2 \cos\varphi + r_1^2 r_2^2} \tag{109}$$

$$\gamma_{\Delta A}(\varphi) = -\frac{r_1 r_2 \sin\varphi}{1 - 2r_1 r_2 \cos\varphi + r_1^2 r_2^2} \tag{110}$$

$$\alpha_{\delta l}(\varphi) = 2k\,\gamma_{\Delta A}(\varphi) \tag{111}$$

$$\alpha_{\Gamma}(\varphi) = -\gamma_{\Delta A}(\varphi) \tag{112}$$

The frequency dependency is contained in the transfer functions H_1, H_2 and H_3. In the case of a detuned frequency, $\varphi \neq 0$, these transfer functions are more complicated than a single pole. However, we can still make a small frequency approximation using a single pole or a zero for frequency much below the cavity pole. In this case we write

$$H_n(s, \varphi) = \begin{cases} 1 + {}^s\!/_{|\omega_n(\varphi)|} & \text{if } \omega_n(\varphi) > 0 \\ 1 & \text{if } \omega_n(\varphi) = 0 \\ \dfrac{1}{1 + {}^s\!/_{|\omega_n(\varphi)|}} & \text{if } \omega_n(\varphi) < 0 \end{cases} \tag{113}$$

where the pole/zero frequencies are given by

$$\omega_1(\varphi) = -2f_{FSR} \frac{1 - 3r_1 r_2 \cos\varphi + r_1^2 r_2^2 (2 + \cos 2\varphi) - r_1^3 r_2^3 \cos\varphi}{1 - r_1 r_2 \cos\varphi - r_1^2 r_2^2 (2 - \cos 2\varphi) + r_1^3 r_2^3 \cos\varphi} \tag{114}$$

$$\omega_2(\varphi) = -f_{FSR} \frac{1 - 2r_1 r_2 \cos\varphi + r_1^2 r_2^2}{1 - r_1 r_2 \cos\varphi} \tag{115}$$

$$\omega_3(\varphi) = -2f_{FSR} \frac{1 - 2r_1 r_2 \cos\varphi + r_1^2 r_2^2}{3 - 2\cos\varphi\, r_1 r_2 - r_1^2 r_2^2} \tag{116}$$

When on resonance, $\varphi = 0$, we get the familiar

$$\gamma_{\delta l}(0) = -\frac{2k r_1 r_2}{1 - r_1 r_2} \tag{117}$$

$$\gamma_{\Delta A}(0) = \alpha_{\delta l}(0) = \alpha_{\Gamma}(0) = 0 \tag{118}$$

$$\omega_1(0) = -\omega_{cav} \quad \text{and} \quad \omega_2(0) = -\sqrt{r_1 r_2}\,\omega_{cav} \tag{119}$$

The transmitted field can be obtained from by replacing r_2 with t_2 in the numerator of the carrier field, i.e.,

$$E_{TRANS}^{cr}(\varphi) = \frac{t_1 t_2}{e^{i\varphi} - r_1 r_2} E_{IN}^{cr} \tag{120}$$

and the above equations for amplitude and phase modulation transfer coefficients stay unchanged. In reflection one has to add the prompt reflected field and the transfer coefficients change significantly,

$$E_{REFL}^{cr}(\varphi) = \left(\frac{t_1^1 r_2}{e^{i\varphi} - r_1 r_2} - r_1\right) E_{IN}^{cr} = \frac{r_2 - r_1 e^{i\varphi}}{e^{i\varphi} - r_1 r_2} E_{IN}^{cr} \tag{121}$$

and

$$\Gamma_{REFL} = \bar{\gamma}_{\delta l}(\varphi)\bar{H}_1(s,\varphi)\delta l + \bar{H}_2(s,\varphi)\Gamma + \bar{\gamma}_{\Delta A}(\varphi)\frac{s}{f_{FSR}}\bar{H}_3(s,\varphi)\Delta A \tag{122}$$

$$\Delta A_{REFL} = \bar{\alpha}_{\delta l}(\varphi)\bar{H}_3(s,\varphi)\delta l + \bar{\alpha}_\Gamma(\varphi)\frac{s}{f_{FSR}}\bar{H}_3(s,\varphi)\Gamma + \bar{H}_2(s,\varphi)\Delta A \tag{123}$$

with

$$\bar{\gamma}_{\delta l}(\varphi) = -2k \frac{r_2 t_1^2 (r_1(1+r_2^2)\cos\varphi - r_2(1+r_1^2))}{(1 - 2r_1 r_2 \cos\varphi + r_1^2 r_2^2)(r_1^2 - 2r_1 r_2 \cos\varphi + r_2^2)} \tag{124}$$

$$\bar{\gamma}_{\Delta A}(\varphi) = \frac{r_1 r_2 t_1^2 t_2^2 \sin\varphi}{(1 - 2r_1 r_2 \cos\varphi + r_1^2 r_2^2)(r_1^2 - 2r_1 r_2 \cos\varphi + r_2^2)} \tag{125}$$

$$\bar{\alpha}_{\delta l}(\varphi) = 2k\,\bar{\gamma}_{\Delta A}(\varphi) \tag{126}$$

$$\bar{\alpha}_\Gamma(\varphi) = -\bar{\gamma}_{\Delta A}(\varphi) \tag{127}$$

and

$$\bar{\omega}_1(\varphi) = -2f_{FSR} \frac{(1 - 2r_1 r_2 \cos\varphi + r_1^2 r_2^2)(r_2(1+r_1^2) - r_1(1+r_2^2)\cos\varphi)}{r_2 - r_1^4 r_2^3 - (2 - \cos 2\varphi)r_1^2 r_2 t_2^2 - r_1(1+r_2^2)(1 - r_1^2 r_2^2)\cos\varphi} \tag{128}$$

$$\bar{\omega}_2(\varphi) = f_{FSR} \frac{(1 - 2r_1 r_2 \cos\varphi + r_1^2 r_2^2)(r_1^2 - 2r_1 r_2 \cos\varphi + r_2^2)}{r_2 t_1^2(r_2(1+r_1^2) - r_1(1+r_2^2)\cos\varphi)} \tag{129}$$

$$\bar{\omega}_3(\varphi) = 2f_{FSR} \frac{t_2^2(1 - 2r_1 r_2 \cos\varphi + r_1^2 r_2^2)}{1 - r_2^2(3 + 3r_1^2 - r_1^2 r_2^2) + 2r_1 r_2(1+r_2^2)\cos\varphi} \tag{130}$$

For a field on resonance we get

$$E_{REFL}^{cr}(0) = \frac{r_2 - r_1}{1 - r_1 r_2} E_{IN}^{cr} \tag{131}$$

$$\bar{\gamma}_{\delta l}(0) = \frac{2kr_2 t_1^2}{(1 - r_1 r_2)(r_2 - r_1)} \tag{132}$$

$$\bar{\gamma}_{\Delta A}(0) = \bar{\alpha}_{\delta l}(0) = \bar{\alpha}_\Gamma(0) = 0 \tag{133}$$

$$\bar{\omega}_1(0) = \omega_{cav}\sqrt{r_1 r_2} \frac{(r_2 - r_1)(1 - r_1 r_2)^2}{r_1 - r_2 + r_1^2 r_2 + r_1 r_2^2 - r_1^3 r_2^2 - r_1^2 r_2^3 + r_1^4 r_2^3 - r_1^3 r_2^4} \tag{134}$$

$$\bar{\omega}_2(0) = \omega_{cav}\sqrt{r_1 r_2} \frac{r_2 - r_1}{r_2 t_1^2} \tag{135}$$

4.2.3 Non-Linear Process

The non-linear process in an OPO involving a seed field is given as $E_{out} = \eta_{OPO} E_{seed}^* E_{pump}$, where η represents the conversion coefficient. Assuming that input fluctuations are small we can

see that the relative amplitude modulation and the phase modulation of each input beam will just appear on the output field. However, the conversion factor is not independent of the field strength, and the phase modulation of the seed field acquires a minus sign at the output due to the fact that $f_{out} = f_{pump} - f_{seed}$. We therefore write

$$\Gamma_{\text{out}} = \Gamma_{\text{pump}} - \Gamma_{\text{seed}} \quad \text{and} \quad \Delta A_{\text{out}} = \Delta A_{\text{pump}} + \Delta A_{\text{seed}} + \cdots \tag{136}$$

Writing the seed and pump fields as

$$E_{seed} = E_{aux}e^{i\Omega t + 2\pi i f_{aux}t + i\phi_{aux}} \quad \text{and} \quad E_{pump} = E_{green}e^{2i\Omega t + i\phi_{green}} \tag{137}$$

the reflected output field can be written as

$$E_{out} = E_{aux2}e^{i\Omega t - 2\pi i f_{aux}t + i(\phi_{green} - \phi_{aux})} \tag{138}$$

with

$$\begin{aligned}
E_{aux2} &= \eta_{OPO} \frac{r_{OR,2}t_{OR,1}}{e^{-2\pi i f_{aux}/f_{O,FSR}} - r_{OR,1}r_{OR,2}} \frac{t_{OR,1}}{e^{2\pi i f_{aux}/f_{O,FSR}} - r_{OR,1}r_{OR,2}} \\
&\quad \times \frac{t_{OG,1}}{1 - r_{OG,1}r_{OG,2}} E_{aux}E_{green} \\
&= \eta_{OPO} \frac{r_{OR,2}t_{OR,1}^2}{1 - 2r_{OR,1}r_{OR,2}\cos(2\pi f_{aux}/f_{O,FSR}) + r_{OR,1}^2 r_{OR,2}^2} \\
&\quad \times \frac{t_{OG,1}}{1 - r_{OG,1}r_{OG,2}} E_{aux}E_{green}
\end{aligned} \tag{139}$$

where *OR* and *OG* represent the red and green OPO parameters, respectively.

In the case of the squeezed field generation we have no seed beam. The green pump beam then generates two correlated red photons for each green photon converted in the process. We write $E_1 E_2 = \eta E_{pump}$. Now setting $E_1 \approx E_2$ we see that the phase of the output field is half of the green input field.

For the SHG we can write $E_{green} = \eta E_{red}^2$ and we see that the phase and amplitude modulation of the red input field simply double at the output, $\Gamma_{\text{green}} = 2\Gamma_{\text{red}}$ and $\Delta A_{\text{green}} = 2\Delta A_{\text{red}} + \cdots$, respectively.

4.2.4 Offset Locking

When two laser beams are interfered and locked with a frequency offset $f_S = f_2 - f_1$, the resulting error signal when demodulated by $\cos\left(2\pi f_S t + \phi_M + \frac{\pi}{2}\right)$ is given by

$$V^{\phi}(s) = \phi_2 - \phi_1 + \phi_M \tag{140}$$

We are omitting the factor $2\sqrt{P_1 P_2}$ which describes the phase-to-power conversion, with P_1 and P_2 the power in each beam, respectively.

5 Compensation Design

The parameters of the feedback compensation network are given in the following tables.

5.1 Laser Locking

Table 5: Parameters for the laser locking servos.

Parameter	Description	Value	Unit
$\alpha_{0,2}$	Pockels modulation index	15	mrad/V
$\alpha_{1,2}$	Pockels modulation index	15	mrad/V
$\alpha_{0,1}$	Main laser PZT input	300	kHz/V
$\alpha_{1,1}$	Aux. laser PZT input	300	kHz/V
$\eta_{QE,0}$	Photodetector quantum efficiency	0.95	
$\eta_{QE,1}$	Photodetector quantum efficiency	0.95	
ε_R	Red photodetector responsivity	0.858	A/W
Z_0	Photodetector transimpedance	40	kΩ
Z_1	Photodetector transimpedance	40	kΩ
P_{PSL}	Power from the PSL	1	mW
P_{Main}	Main laser power	500	mW
P_{Aux}	Auxiliary laser power	50	mW
f_{Aux}	Auxiliary laser frequency offset	29.507	MHz
$\eta_{PSL,0}$	Attenuation factor of PSL beam	0.5	
$\eta_{Main,0}$	Attenuation factor of main beam	0.002	
$\eta_{Main,1}$	Attenuation factor of main beam	0.002	
$\eta_{Aux,1}$	Attenuation factor of aux. beam	0.01	
g_0	Overall gain	0.022	
$g_{0,1}$	Fast path gain	32000	
$g_{0,2}$	Pockels cell path	240	
$f_{0,Z1}$	Zero in electronics	0	kHz
$f_{0,Z2}$	Zero in electronics	77.6	kHz
$f_{0,Z3}$	Zero in electronics	97.5+205i	kHz
$f_{0,Z4}$	Zero in electronics	97.5–205i	kHz

$f_{0,Z5}$	Zero in electronics	10000	kHz
$f_{0,P1}$	Pole in electronics	1	kHz
$f_{0,P2}$	Pole in electronics	2.13	kHz
$f_{0,P3}$	Pole in electronics	3.1	kHz
$f_{0,P4}$	Pole in electronics	150	kHz
$f_{0,P5}$	Pole in electronics	100	kHz
$f_{0,P6}$	Pole in electronics	10	kHz
$f_{0,P7}$	Pole in electronics	23	kHz
$f_{0,P8}$	Pole in electronics	0.01	kHz

5.2 SHG and OPO

Table 6: Parameters for the SHG length servo.

Parameter	Description	Value	Unit
η_4	Fraction of detected power	0.2	
$\eta_{QE,4}$	Photodetector quantum efficiency	0.95	
Z_4	Photodetector transimpedance	1000	Ω
f_4	Photodetector pole	5	MHz
α_4	PZT displacement coefficient	5	nm/V
g_4	Servo gain	31,600,000	
$f_{4,Z1}$	Zero in electronics	500	Hz
$f_{4,P1}$	Pole in electronics	1	Hz
$f_{4,P2}$	Pole in electronics	1	Hz

Table 7: Parameters for the OPO length servo.

Parameter	Description	Value	Unit
η_5	Fraction of detected power	0.002	
$\eta_{QE,5}$	Photodetector quantum efficiency	0.95	
Z_5	Photodetector transimpedance	200	Ω
f_5	Photodetector pole	10	MHz

α_5	PZT displacement coefficient	5	nm/V
g_5	Servo gain	10,000,000	
$f_{5,Z1}$	Zero in electronics	500	Hz
$f_{5,P1}$	Pole in electronics	1	Hz
$f_{5,P2}$	Pole in electronics	1	Hz

5.3 Coherent Locking and Local Oscillator

Table 8: Parameters for the coherent locking servo.

Parameter	Description	Value	Unit
$\eta_{QE,2}$	Photodetector quantum efficiency	0.95	
Z_2	Photodetector transimpedance	1000	Ω
η_2	Attenuation factor in path to S_2	0.01	
f_2	Photodetector pole	10	MHz
$\alpha_{2,1}$	PZT displacement coefficient	5	nm/V
$\alpha_{2,2}$	Auxiliary laser additive offset	1	V/V
$g_{2,0}$	Servo common gain	320,000	
$g_{2,1}$	Servo PZT gain	1,000,000	
$g_{2,2}$	Servo additive offset gain	7.08	
$f_{2,Z1}$	Zero in common path electronics	20	kHz
$f_{2,Z2}$	Zero in common path electronics	20	kHz
$f_{2,P1}$	Pole in common path electronics	1	kHz
$f_{2,P2}$	Pole in common path electronics	1	kHz
$f_{2,P3}$	Pole in common path electronics	40	Hz
$f_{2,P4}$	Pole in PZT path electronics	10	Hz
$f_{2,Z3}$	Zero in additive offset path	0	Hz
$f_{2,Z4}$	Zero in additive offset path	0	Hz
$f_{2,P5}$	Pole in additive path electronics	5	Hz
$f_{2,P6}$	Pole in additive path electronics	5	Hz

Table 9: Parameters for the local oscillator locking servo.

Parameter	Description	Value	Unit
$\eta_{QE,3}$	Photodetector quantum efficiency	0.95	
Z_3	Photodetector transimpedance	1000	Ω
$\eta_{Aux,3}$	Attenuation factor in aux. path to S_3	0.01	
$\eta_{LO,3}$	Attenuation factor in LO path to S_3	0.01	
P_{LO}	Power in the LO	10	mW
f_3	Photodetector pole	5	MHz
$\alpha_{3,1}$	PZT displacement coefficient	5	nm/V
$\alpha_{3,2}$	Main laser additive offset	1	V/V
$g_{3,0}$	Servo common gain	100,000	
$g_{3,1}$	Servo PZT gain	1,000,000	
$g_{3,2}$	Servo additive offset gain	7.08	
$f_{3,Z1}$	Zero in common path electronics	20	kHz
$f_{3,Z2}$	Zero in common path electronics	20	kHz
$f_{3,P1}$	Pole in common path electronics	1	kHz
$f_{3,P2}$	Pole in common path electronics	1	kHz
$f_{3,P3}$	Pole in common path electronics	40	Hz
$f_{3,P4}$	Pole in PZT path electronics	10	Hz
$f_{3,Z3}$	Zero in additive offset path	0	Hz
$f_{3,Z4}$	Zero in additive offset path	0	Hz
$f_{3,P5}$	Pole in additive path electronics	5	Hz
$f_{3,P6}$	Pole in additive path electronics	5	Hz